

Mean Motion Resonances in the Trans-neptunian Region

I. The 2:3 Resonance with Neptune

D. Nesvorný¹ and F. Roig

Institute of Astronomy and Geophysics, São Paulo University, Av. Miguel Stefano 4200, 04301 São Paulo, SP, Brazil

E-mail: david@obs-nice.fr

Received December 8, 1999; revised June 9, 2000

The stability of the 2:3 mean motion resonance with Neptune is systematically explored and compared to the observed resonant population. It is shown that orbits with small and moderate amplitudes of the resonant angle are stable over the age of the Solar System. The observed resonant population is distributed within the stability limits. There exists an interval of large resonant amplitudes, where orbits are marginally unstable. Resonant objects starting in this interval may leave the resonance by slow increase of their resonant amplitudes on a time scale of several billion years. These objects eventually attain Neptune-crossing trajectories and contribute to the flux of Jupiter-family comets. The number of objects leaking from the 2:3 resonance per time interval is calibrated by the number of objects needed to keep the Jupiter-family comets population in steady state. This allows us to compute the upper limit of the number of resonant objects with cometary size. The effects of collisions and mutual gravitational scattering are discussed in this context. © 2000 Academic Press

Key Words: Kuiper Belt objects; celestial mechanics.

1. INTRODUCTION

Edgeworth (1949) and Kuiper (1951) suggested that the Solar System extends beyond Neptune in the form of a belt of small bodies. Later, when Fernández (1980) proposed that such a belt (hereafter we refer to the belt as the Kuiper Belt—KB) can be a reservoir of Jupiter-family comets, the interest in providing the direct observational evidence of the belt increased. The discovery of 1992 QB1 by Jewitt and Luu (1993) was soon succeeded by other observations and now the number of known Kuiper Belt objects (KBOs) is nearly 200.

The stability of the trans-Neptunian region has been numerically studied by Levison and Duncan (1993) and Holman and Wisdom (1993). Their results were extended by Duncan *et al.* (1995) who computed a detailed map of stable/unstable regions

in the KB by integrating a large number of orbits in the 32–50 AU semi-major axis interval over 4×10^9 years. The orbits starting at perihelion distances q less than 35 AU were found unstable unless they were associated with some mean motion resonance (MMR) with Neptune. The orbits with $q > 35$ AU were found stable unless they were related with perihelion or node secular resonances (mainly ν_8 , ν_{17} , and ν_{18} located at $40 < a < 42$ AU according to Knežević *et al.* 1991).

There was no similar work published until now on the stability of the asteroid belt over the age of the Solar System due to the relatively short orbital periods of asteroids and the necessity to use a short time step in their simulations. If the effect of inner planets (Venus to Mars) also has to be taken into account, the time step of asteroid simulation is a factor of 25 smaller than what is used for the KB; i.e., the computational need for a 4×10^9 -year simulation in the KB is roughly equal to the computational need of a $\frac{4}{7} \frac{4 \text{ Byr}}{25} = 90$ Myr simulation in the asteroid belt (the factor 4/7 accounts for seven planets used in the asteroid belt against four planets used in the KB).

Nevertheless, considerable progress has been made on the long-term stability of asteroidal orbits using a different approach. In this approach, the chaotic evolution of asteroid orbital elements (and secular frequencies) is numerically computed on the time interval covered by simulation (usually not exceeding 10^8 years) and then the expected chaotic evolution of orbits on a longer time interval is estimated. Orbits are judged to be stable if the chaotic change of orbital elements (or frequencies) extrapolated to 4×10^9 years is small. There is no practical need for studying the stability of minor bodies with the current configuration of planets on longer time spans as the planetary orbits and physical conditions have been substantially different during the Solar System formation.

In particular, the simulated time interval is usually divided in several sub-intervals and the motion is approximated by a quasi-periodic evolution (which would be an exact solution of the integrable system) on each of them. This quasi-periodic approximation can be either explicitly computed (Laskar 1999) or one can rely only on the evaluation of motion integrals.

¹ Present address: Observatoire de la Côte d'Azur, BP. 4229, Bd. de l'Observatoire, 06304 Nice Cedex 4, France.

The integrals of motion are either *proper* orbital elements or *proper* frequencies depending on their physical meaning. The change in the proper elements and frequencies between consecutive sub-intervals is due to the chaoticity of motion and is frequently referred to as the *chaotic diffusion*. The local rate of chaotic diffusion is then closely related to the orbital stability and simple models have been devised in specific cases (Murray and Holman 1997).

We use in the following the approach of Laskar (1994) and Morbidelli (1996) who define the motion integrals as either the extrema or average of orbital elements computed on the sub-intervals. This method allows for the detection of slow chaotic evolution of orbits and additionally has a clear astronomical interpretation. The relative change in frequencies (Laskar 1988, 1999) is also a widely used indicator of the rate of chaotic diffusion. The computation of frequencies usually permits the identification of resonances responsible for chaos.

Another useful tool for the determination of the orbital stability/instability is the maximum Lyapunov Characteristic Exponent (LCE) which measures the rate of divergence of nearby trajectories. It is defined as $\lim_{t \rightarrow \infty} \ln \Delta(t)/t$, where $\Delta(t)$ is the norm of the variational vector at time t (Oseledec 1968, Benettin *et al.* 1976). Although the relationship of the LCE to the chaotic diffusion and the orbital stability is a complicated problem (Morbidelli and Froeschlé 1995), evaluation of the LCE frequently helps in identifying the most evident irregular and possibly unstable orbits. It is also clear that orbits with a very small LCE are likely to be stable over long time intervals.

This paper deals with the 2:3 MMR with Neptune. This resonance is of special interest as from 191 KBOs currently registered in the Asteroid Orbital Elements Database of the Lowell Observatory (September 1999—<ftp://ftp.lowell.edu/pub/elgb/astorb.html>), 68 objects fall within a small semi-major axis interval around 39.45 AU, where this resonance is centered. This resembles the situation in the outer asteroid belt ($3.27 < a < 4.5$ AU), where from 258 numbered asteroids some 120 objects known as the Hilda group are situated in the 3:2 MMR with Jupiter. In both cases the resonant space is populated more densely than the neighboring non-resonant space; this is usually believed to be a consequence of the Solar System early evolution (Malhotra 1995, Liou and Malhotra 1997, Hahn and Malhotra 1999).

The long-term stability of Pluto's 2:3 resonant orbit has been confirmed in numeric simulations of Kinoshita and Nakai (1984) and Sussman and Wisdom (1988). It turned out that despite a positive LCE ($\sim 10^{-7}$ year $^{-1}$) Pluto's orbit is stable over the age of the Solar System.

Concerning the global stability of the 2:3 Neptune MMR, the works based on averaged circular (Morbidelli *et al.* 1995) and non-averaged circular (Malhotra 1996) models indicated that the central resonant space is stable, but both were missing an important ingredient—complete perturbations of the outer giant planets other than Neptune—in order to provide sufficiently reliable stability boundaries.

Denoting the resonant angle of the 2:3 Neptune MMR by

$$\sigma = 2\lambda_N - 3\lambda + \varpi, \quad (1)$$

where λ and ϖ are the mean and perihelion longitudes and λ_N is the mean longitude of Neptune, the resonant motion is characterized by oscillation of σ around 180° . This oscillation is alternatively called the *libration* as opposed to the non-resonant situation where σ circulates. In the case of Pluto the amplitude of σ libration (A_σ) is about 82° . Additionally, Pluto is known to reside in the Kozai secular resonance, where the argument of perihelion ω librates about 90° with an amplitude (A_ω) of 22° .

The stability boundaries in the 2:3 Neptune MMR as a function of the resonant amplitudes A_σ and A_ω were computed by Levison and Stern (1995). They found that for inclinations similar to Pluto's inclination ($\sim 17^\circ$) the orbits starting with $A_\sigma < 50^\circ$ were stable and the orbits with $A_\sigma > 120^\circ$ were unstable over 4×10^9 years. For intermediate A_σ , usually a small A_ω was needed for orbital stability. Similarly, Duncan *et al.* (1995) have shown that the motion at $e = 0.2$ is stable over the age of the Solar System provided that $A_\sigma < 70^\circ$. The stability of the 2:3 MMR was further investigated by Morbidelli (1997) with an additional concern in the number of escaping objects and their relation to Jupiter-family comets. This later work confirmed the finding of Duncan *et al.* (1995) that the chaotic evolution on the margin of stable region mostly affects A_σ .

We investigate the 2:3 resonant dynamics aiming our study at a detailed and global understanding of chaotic and regular motions inside this resonance. Our approach closely follows the work of Nesvorný and Ferraz-Mello (1997b). In Section 2, we describe the setup of numerical experiments. The dynamics of the 2:3 Neptune MMR at low inclinations is discussed in Section 3. We identify several interior resonances responsible for chaos and estimate the time scales on which they destabilize orbits. Based on this analysis we determine the extent of the region from which bodies are currently leaking to Neptune-crossing orbits (Section 4). Then we scale the escape rate to get the correct number of Jupiter-family comets and constrain the current resonant population (Section 5). The effect of collisions and dynamic scattering within the resonance is studied by a simple model in Section 6. In Section 7, we extend the present study by exploring the orbital dynamics at large inclinations. Finally, we discuss the orbits of observed KBOs in the 2:3 Neptune MMR (Pluto and Plutinos) in Section 8.

This paper is the first part of the work that collects our results on the mean motion resonances in the Kuiper Belt. The second paper (Nesvorný and Roig 2000) is devoted to the 1:2 and 3:4 Neptune MMRs and the global structure of MMRs in the 35- to 50-AU semi-major axis interval.

2. THE SET-UP OF NUMERICAL EXPERIMENTS

The resonant value of the semi-major axis is $a_{\text{res}} = 39.45$ AU. The resonant dynamics are characterized by coupled oscillations

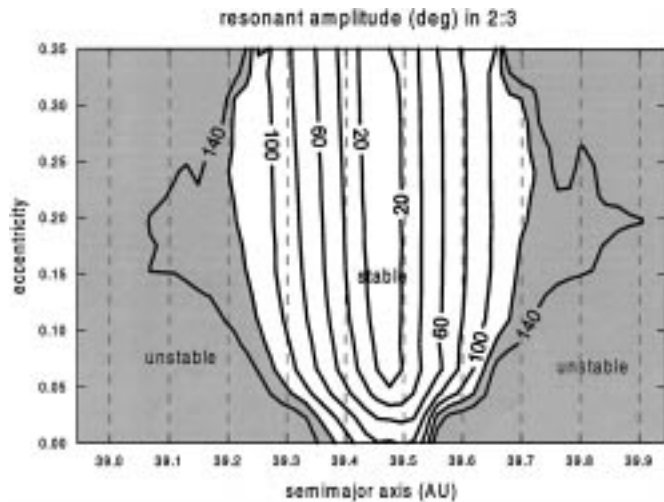


FIG. 1. The resonant amplitude A_σ (in degrees) of the 2:3 Neptune MMR. The gray area roughly corresponds to the strongly unstable motion at $A_\sigma > 120^\circ$ (Morbidelli 1997).

of the semi-major axis about a_{res} and of σ (Eq. 1) about 180° with a typical period of 20,000 years. We also recall that other important characteristics of the 2:3 MMR is the presence of the Kozai resonance (at $e = 0.25$ for small A_σ —Morbidelli *et al.* 1995). This secular resonance concerns libration of ω around 90° or 270° and forces coupled variations of the e and i with a typical period of several million years.

According to numerical simulations (Duncan *et al.* 1995, Morbidelli 1997) the orbits in the 2:3 MMR with the libration amplitude A_σ larger than about 120° are unstable in relatively short time intervals. In Fig. 1 we show the dependence of A_σ on a and e . The amplitudes have been computed numerically for small i and initial $\sigma = 180^\circ$ in a model with four outer planets. The maximum excursion of σ from 180° in 10^6 years was taken as A_σ .

The grey region in Fig. 1 schematically delimits strongly unstable orbits for $A_\sigma > 120^\circ$. As we show later, the actual size of the stable resonant region is somewhat smaller than the central white area in Fig. 1 due to the presence of secular resonances and the possibility of close approaches to Uranus at large e . More-

over, also the range of a corresponding to motions stable over 4×10^9 years covers a somewhat smaller interval than that indicated in Fig. 1. There exists an interval of marginal instability at about 100° – 120° (we define the marginally unstable region and specify its range more precisely in Section 4), where the chaotic evolution, although slow, is sufficient to enlarge A_σ beyond 120° (i.e., to the strongly unstable amplitudes) in less than 4×10^9 years.

Following the approach used in studies of the first-order jovian resonances in the main asteroid belt (Ferraz-Mello 1994, Nesvorný and Ferraz-Mello 1997b), we calculate the maximum LCE and estimate the rate of chaotic diffusion for orbits on a regular grid of initial actions a , e , i .

We have run simulations for two sets of initial actions:

- (1) 1010 test particles with $38.8 \leq a \leq 39.8$ AU ($\Delta a = 0.01$ AU), $e = 0.01, 0.05, 0.1, 0.15, 0.2, 0.23, 0.25, 0.27, 0.3, 0.35$ (101 test particles at each e), and $i = 5^\circ$;
- (2) 405 test particles with $a = 39.41$ AU, $0 \leq e \leq 0.4$ ($\Delta e = 0.005$), and $5^\circ \leq i \leq 25^\circ$ ($\Delta i = 5^\circ$, 81 test particles at each value of i).

In the first set we explore the resonant orbits with small i and in the second set we study the dynamics at large i .

The initial angles of test particles were chosen so that $\sigma = 180^\circ$, $\omega = 90^\circ$, and $\Omega - \Omega_P = 0$, where Ω and Ω_P are the node longitudes of a test particle and Pluto, respectively. In this way, the plane of initial conditions intersects the libration centers of both the 2:3 and Kozai resonances.

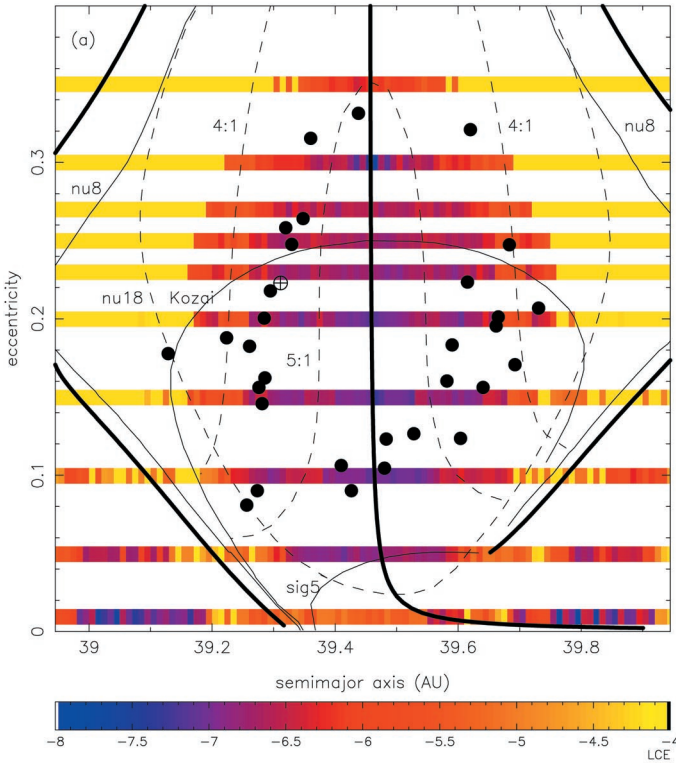
In both runs the test particles were numerically integrated with four outer planets (Jupiter to Neptune) for 10^8 years by the symmetric multi-step integrator (Quinlan and Tremaine 1990). The initial conditions of the planets were chosen at their positions at JD 2449700.5 with respect to the ecliptic plane and equinox at epoch J2000. The time steps of 40 days for the planets and 200 days for the test particles were used. In the course of integration, a run-time digital filter (Quinn *et al.* 1991) was applied to $a \exp i\sigma$, $e \exp i\varpi$, and $i \exp i\Omega$ ($i = \sqrt{-1}$), and the initial sampling of 5 years was augmented to 2500 years without introducing fake frequencies in the Fourier spectrum (the problem of frequency aliasing is described in Press *et al.* 1992).

FIG. 2. The estimate of the maximum LCE (a) and the minimum distance to Neptune (b) in the 10^8 year numerical simulation of orbits in the 2:3 Neptune MMR. The initial inclinations were 5° . See text for the description of other initial elements of the test particles. The separatrices (bold border lines), libration centers (bold vertical line at 39.45 AU), and the main inner resonances (Kozai and ν_8 are denoted by full thin lines; ν_{18} , 4:1, and 5:1 three-body resonances are dashed; the secondary 5:1 resonance at $e < 0.05$ is denoted by sig5) were computed by a semi-numerical method. The test particles escaping from the 2:3 resonance before the end of the integration (in yellow) have simultaneously large LCE estimates and small minimum distances from Neptune. The most regular orbits, with $\text{LCE} \leq 10^{-6.5} \text{ year}^{-1}$, are located in the interval of about 0.3 AU centered at the libration centers and have eccentricities between 0.05 and 0.3 (blue/dark red in (a)). There are no regular orbits above $e = 0.35$ due to the overlap of ν_8 and ν_{18} . The best angular protection against approaches to Neptune happens at the libration centers for $0.2 < e < 0.35$ where the minimum distance is larger than 15 AU. The orbital elements of known Plutinos (large dots) and Pluto (\oplus) were taken from Nesvorný *et al.* (2000).

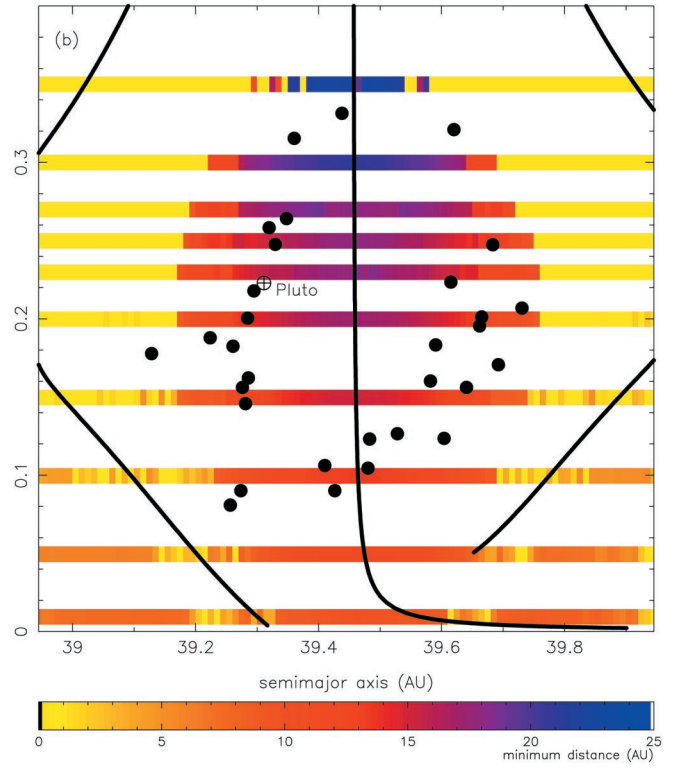
FIG. 8. (a) The estimate of the maximum LCE in the 2:3 Neptune MMR. (b) The minimum distance to Neptune. The initial a was chosen at 39.41 AU, which corresponds to $A_\sigma \sim 60^\circ$. See text for the definition of other initial elements. The separatrices (full lines) and libration centers (dashed line) of the Kozai resonance were computed for $A_\sigma = 0$. The orbital elements of known Plutinos (large dots) and Pluto (\oplus) are shown.

2

LCE

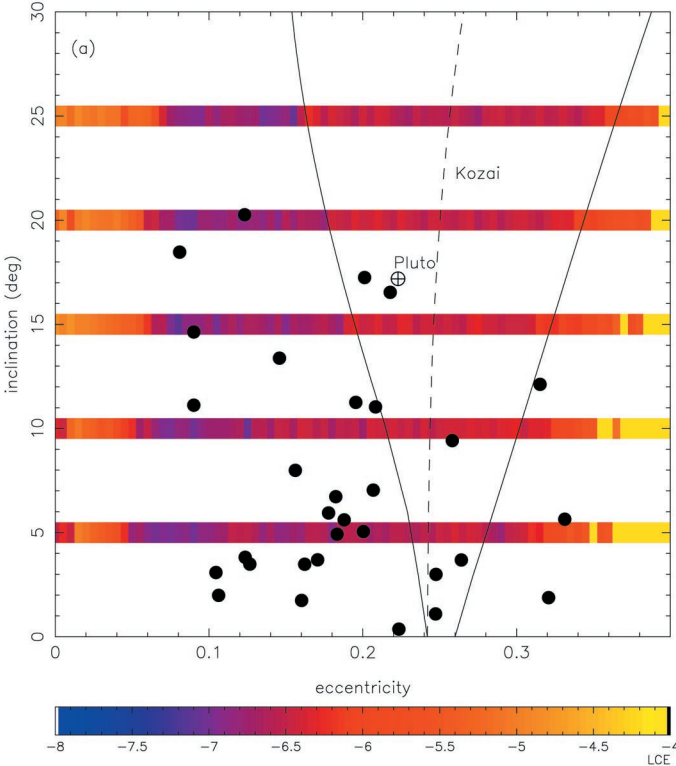


minimum distance from Neptune

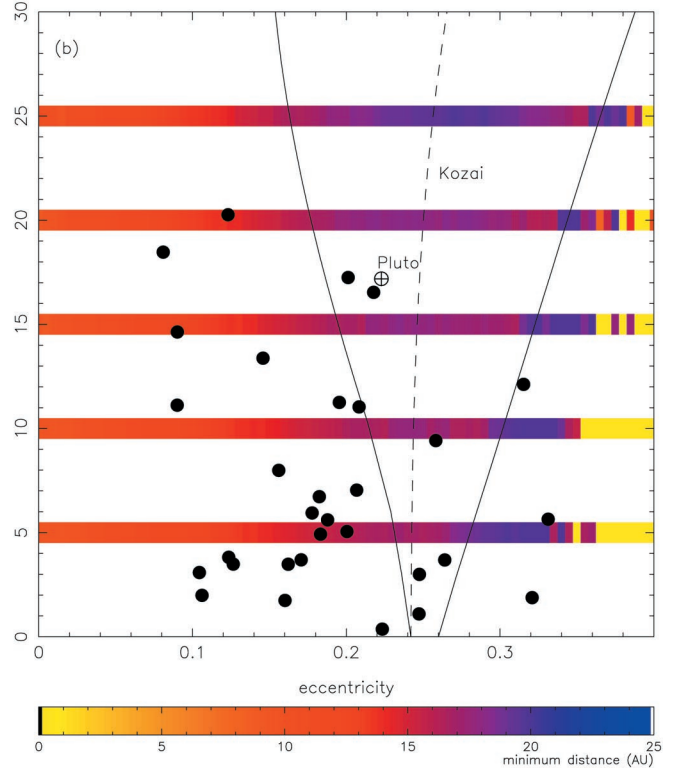


8

LCE



minimum distance from Neptune



The actual procedure consisted of a consecutive application of time-domain FIR filters (Press *et al.* 1992). First, one filter (filter A) was used two times increasing the sampling by a factor of 100 and then a second filter (filter B) was additionally applied, increasing the sampling by a factor of 5. See Nesvorný and Ferraz-Mello (1997a) for the specifications of both filters. With this procedure, all periods smaller than 5000 years were suppressed and all periods larger than 10^4 years were retained. In addition to the equations of motion, the variational equations also were numerically integrated using the symmetric multi-step method. The variational vector was periodically renormalized in order to avoid the computer overflow (Benettin *et al.* 1976). This allowed us to estimate the maximum LCE for all test particles.

3. THE LOW-INCLINATION RUN

3.1. The Maximum LCE

The estimate of the maximum LCE for each test particle was computed as $\ln \Delta(t)/t$ with $t = 10^8$ years, and was plotted as a function of a and initial e in Fig. 2a for the first set of initial conditions. We have compensated in this figure for short-period variations by a shift of 0.145 AU in a so that the test particles with smallest A_σ are near the true libration center at 39.45 AU. This shift mainly accounts for the difference between the instantaneous initial a and its average over the orbital period of Jupiter. This difference is about the same for all test particles (except at very small e where the location of the true libration center strongly depends on a). Such correction was not introduced for e (and i) which was less affected by the short-period variations and which had initial values within 0.01 (and 2°) of their averages over 10^7 years. In Fig. 2b, the minimum distances of test particles to Neptune in 10^8 years are shown.

The color coding in Fig. 2a was chosen so that *yellow* corresponds to the initial conditions of test particles that escaped to Neptune-crossing orbits in the integration time span; *red* corresponds to the initial conditions for which the estimate of the LCE on 10^8 years clearly converges to its limit value and the corresponding orbits have non-zero LCEs. *Blue* corresponds to the initial conditions of the most regular orbits. For these, there was no (evident) convergence to a non-zero value and $\log(\ln \Delta(t)/t)$ linearly decreased with $\log t$, even if in many cases there appeared characteristic cusps indicating local hyperbolic structures in the phase space (Morbidelli and Nesvorný 1999).

In Fig. 2, we plot the separatrices and libration centers of the 2:3 MMR and several secular resonances, which were found inside the 2:3 MMR: ν_8 (the 1:1 commensurability of the mean perihelion frequencies of a minor body and Neptune—full line near separatrices marked nu8), ν_{18} (the 1:1 commensurability of the mean nodal frequencies of a minor body and Neptune—dashed line marked nu18), and the Kozai resonance (the 1:1 commensurability of the mean perihelion and node frequencies of a minor body—full line intersecting the libration center at $e = 0.25$, marked Kozai). Also the secondary resonance is shown where the frequency of σ is a factor of 5 larger than the frequency

of the perihelion longitude (full line at $e < 0.05$ marked sig5). Other secondary resonances, where the ratios of the resonant and perihelion frequencies are smaller, are located at very small e . The location of all these inner resonances in the 2:3 MMR and their effects on long-term dynamics of resonant bodies has been known since Morbidelli (1997).

Apart from the above inner resonances, we have calculated the commensurabilities between the resonant frequency and the frequency of Uranus–Neptune quasi-resonance, i.e., the frequency of the angle $\lambda_U - 2\lambda_N$ that circulates with a negative derivative and the period of 4230 years. This type of resonance involving two perturbing bodies and a minor body was recently shown important in clearing the 2:1 MMR with Jupiter and opening the Hecuba gap at $a = 3.27$ AU in the asteroid belt (Ferraz-Mello *et al.* 1998). We plot the commensurabilities 4:1 and 5:1 between the resonant frequency and $1/4230 \text{ year}^{-1}$ in Fig. 2a (dashed lines marked 4:1 and 5:1).

At these “three-body” resonances, the LCE is moderately larger than in the background. While the 4:1 resonance has the LCE about $10^{-5.6} \text{ year}^{-1}$, more than a factor of 10 larger than in the background, the 5:1 resonance is weaker, with the LCE rising from the background by a factor of $10^{0.5}$. Although the contrast of paper-printed version of Fig. 2a is not as good as on the computer screen, one can note that the anomalous LCE value follows the lines of the 4:1 and 5:1 resonances proving them to be important for orbital dynamics on long time scales.

The inner resonance locations in the 2:3 Neptune MMR were computed by the semi-numerical method of Henrard (1990) in a frame of the averaged, spatial ($i \neq i_N = 0$) and circular ($e_N = 0$) models. As the full exposition of this method goes beyond the scope of this paper, we refer the reader to Moons *et al.* (1998), where the description of its application to MMRs can be found.

The extent of regular and weakly chaotic trajectories is clearly delimited in Fig. 2a and corresponds to the orbital elements plotted in blue and dark red. The corresponding resonant orbits stay phase-protected from close encounters with Neptune in the whole integrated time interval (Fig. 2b). The central resonant area is enclosed by the ν_8 and ν_{18} secular resonances which overlap and generate strong chaos at, otherwise stable, large A_σ . The upper eccentricity limit of the blue/dark red region at about 0.35 coincides with the lower limit of chaos generated by this overlap, and moreover, for $e > 0.35$ the secular oscillations of e drive orbits to approach Uranus at distances less than 5 AU ($a_U = 19.22$ AU).

The orbits starting at $A_\sigma > 130^\circ$ are usually fast driven (in at most several 10^7 years) to the borders of the 2:3 MMR. There, while σ alternates between libration and circulation, the test particles’ eccentricities chaotically evolve toward the Neptune-grazing limit ($e \sim 0.2$) or, if e ’s are already initially large, the particles suffer close encounters with Neptune and are extracted from the resonance. This is the typical fate of the test particles; their initial orbital elements are shown in yellow in Fig. 2.

Conversely, for orbits starting with $A_\sigma < 100^\circ$ and $0.05 < e < 0.25$ (note that this limit is eccentricity dependent for larger e :

$A_\sigma < 60^\circ$ for $e = 0.3$, and reduces to zero for $e = 0.35$), the LCE decreases with time nearly to $10^{-7} \text{ year}^{-1}$ showing in many cases no strong tendencies to converge. This however depends on exact values of initial a and e . For $0.1 < e < 0.2$, the 5:1 three-body resonance influences orbits with $A_\sigma \sim 60^\circ$ and makes their LCE converge to about $10^{-6.7} \text{ year}^{-1}$. For most other initial A_σ and $e < 0.2$, $\log \ln \Delta(t)/t$ linearly decreases with $\log t$ with frequent “cusps” typical for the situation, where the trajectory passes close to hyperbolic resonant points. Although we do not identify the true nature of weak resonances responsible for this behavior (a detailed identification would be literally a watchmaker’s work in view of the number of frequencies present in the problem), it may be expected that the convergence of $\ln \Delta(t)/t$ toward a positive value happens in an extended simulation. Our guess is that the measure of trajectories in the 2:3 Neptune MMR with $e < 0.2$ having the LCE smaller than $10^{-8} \text{ year}^{-1}$ is very small.

Concerning $e > 0.2$ and small to moderate A_σ , one can discern a reddish color at the corresponding initial conditions in Fig. 2a. This is a consequence of the fact that $\ln \Delta(t)/t$ converges to its asymptotic value which is larger than $10^{-6.8} \text{ year}^{-1}$. Apart from the 5:1 three-body resonance, it is the Kozai resonance that causes the chaos there, because the initial conditions were chosen so that its center at 90° and the corresponding libration space could be sampled. The Kozai resonance is narrow for small inclinations ($\Delta e \sim 0.05$ for $i = 5^\circ$) and as we have noticed in the simulation the test particles with $i = 5^\circ$ almost never remain for a long time with stable ω librations. Their ω typically alternates between circulation and libration on the time scale of several million years. This behavior results in the positive LCE, of about $10^{-6.6} \text{ year}^{-1}$, calculated in our simulation for the test particles starting near $e = 0.25$.

The resonant space available for regular motion (we use the word “regular” as a synonym for “weakly chaotic” rather than to refer to true regularity in the sense of zero LCE) shrinks for $e > 0.25$ and disappears for $e = 0.35$. As shown in Fig. 2a, the most regular behavior happens at $e = 0.3$, above the Kozai and below the 5:1 resonances, and a very small A_σ .

On the boundary between the escaping (yellow) and regular (blue) orbits, a number of initial conditions in an interval of some 0.1 AU in a have an intermediate value of the LCE (10^{-6} – $10^{-5} \text{ year}^{-1}$, light red in Fig. 2a). We have noticed that these orbits chaotically evolve in 10^8 years, which suggests that they might be destabilized in longer time intervals (for this, it is sufficient to rise their A_σ above 120° – 130°). The simulations of Morbidelli (1997) showed the existence of such process. We refer to this interval as the “marginally unstable region.”

At this point we would like to draw the reader’s attention to the inner structure of the marginally unstable region. The 4:1 three-body resonance plays an important role here. For $e = 0.15$, this resonance furnishes a “smooth” passage between the weakly chaotic ($A_\sigma < 110^\circ$) and escaping ($A_\sigma > 130^\circ$) orbits. For $e = 0.2$ the situation slightly changes as the 4:1 resonance (now approximately at $105^\circ < A_\sigma < 120^\circ$) is separated from the

escaping initial conditions with $A_\sigma > 130^\circ$ by a narrow interval of weakly chaotic motion (at $120^\circ < A_\sigma < 130^\circ$). This latter region, however, does not act as a true barrier in the phase space (Section 4). Although slightly retarding the evolution from the 4:1 resonance to $A_\sigma > 130^\circ$, orbits can efficiently “leak” through this region to larger A_σ . The 4:1 three-body resonance joins the escaping region at $e = 0.3$. All orbits with $A_\sigma > 110^\circ$ are unstable within 10^8 years, and already for $A_\sigma = 70^\circ$ the orbital elements are visibly irregular suggesting the enlargement of the marginally unstable area at $e = 0.3$.

The minimum distance from Neptune (Fig. 2b) ranges between 7 and 25 AU for those test particles surviving 10^8 years in the resonance. While for $e \sim 0.05$ – 0.1 , the minimum distances are as low as 10 AU, for $e = 0.3$ and small A_σ the resonant–protection mechanism assures a 20 AU separation from Neptune. This is a consequence of resonant bodies having conjunctions with Neptune at aphelion of their orbits and the fact that more elongated orbits have larger aphelion distances (Nesvorný and Roig 2000). For example, $a_{\text{res}}(1 + e) - a_N = 17.3$ AU for $e = 0.2$, which is in good agreement with the numeric result for $A_\sigma = 0$ in Fig. 2b.

In both panels of Fig. 2 we show the semi-major axis and eccentricity of Pluto (\oplus) and Plutinos (large dots) at the intersection of their trajectories with $\sigma = 180^\circ$ and $\omega = 90^\circ$. These data were taken from Nesvorný *et al.* (2000) and reflect the knowledge of Plutinos’ orbital distribution in March 1999 (Minor Planet Center Orbital Database, <http://cfa-www.harvard.edu/cfa/ps/lists/TNOs.html>). In brief, Nesvorný *et al.* (2000) performed a numeric simulation of 33 Plutinos (and Pluto) and determined their smoothed orbital elements at the moment when $\sigma = 180^\circ$ and $\omega = 90^\circ$ simultaneously. Advancing the orbital elements to this manifold is well suited for the present comparison as the initial conditions in Fig. 2 also have $\sigma = 180^\circ$ and $\omega = 90^\circ$. There is one symbol per body in Fig. 2 corresponding to the first intersection with the manifold. Due to the symmetry of the 2:3 MMR with respect to the libration centers, the next intersection of a trajectory with $\sigma = 180^\circ$ would be symmetrically placed on the opposite side of the libration centers.

The distribution of Plutinos in the (a, e) -plane samples the region $39.25 < a < 39.7$ AU and $0.08 < e < 0.34$ which corresponds reasonably well with the extension of the central regular region of the 2:3 MMR. There are two regions in Fig. 2 that look relatively unpopulated. The first one is in the center of the 2:3 MMR at $39.35 < a < 39.6$ AU and $0.15 < e < 0.3$. Here, according to Nesvorný *et al.* (2000), the libration amplitudes of Plutinos could have been excited by Pluto’s gravitational sweeping effect.

The second unpopulated region is located at $0.05 < e < 0.08$. At these eccentricities, orbits are unaffected by the chaos under the 5:1 secondary resonance, where the 2:1, 3:1, and 4:1 secondary resonances and ν_{18} are simultaneously present. In fact, no resonant objects are known with $e < 0.08$. We return to this issue in Section 8.

3.2. The Chaotic Evolution of Actions and Frequencies

To measure the chaotic evolution of orbital elements we have computed, for each integrated test particle, the maxima of filtered σ , e , and i on two consecutive intervals of 45 Myr each (i.e., the total length of 90 Myr). These quantities do not change with time in the case of quasi-periodic motion. We used a larger window interval (45 Myr) than Morbidelli (1997; 10 Myr) expecting to improve the accuracy.

The following quantities were computed,

$$\begin{aligned}\delta A_\sigma &= \left| \sigma_{\max}^{(2)} - \sigma_{\max}^{(1)} \right| \\ \delta e &= \left| e_{\max}^{(2)} - e_{\max}^{(1)} \right| \\ \delta i &= \left| i_{\max}^{(2)} - i_{\max}^{(1)} \right|\end{aligned}\quad (2)$$

where the indexes 1 and 2 refer to maxima obtained in the first and second intervals, respectively. In addition, we smoothed the above quantities over initial conditions with the same e by a 5-point (0.048 AU) running window in a . The resulting smoothed values of δA_σ (Fig. 3a), δe (Fig. 3b), and δi (Fig. 3c) show how much the orbital elements change, on average, due to the chaotic evolution of trajectories on the time interval of 45 Myr.

To measure the chaotic evolution of frequencies we used frequency analysis (Laskar 1999). The frequencies f_σ , f_ϖ , and f_Ω were determined from the Fourier spectra of $a \exp i\sigma$, $e \exp i\varpi$ and $i \exp i\Omega$, respectively, on two consecutive intervals of 45 Myr using the algorithm of Frequency Modified Fourier Transform (FMFT₂; Šidlichovský and Nesvorný 1997). While for f_ϖ and f_Ω this meant the determination of the leading peak frequency in the spectra of $e \exp i\varpi$ and $i \exp i\Omega$, respectively, the technical procedure for f_σ was somewhat more involved due to the large number of terms with similar amplitude in the Fourier spectrum of $a \exp i\sigma$.

The resonant, perihelion, and node frequencies determined in this way do not change with time in the case of quasi-periodic motion and change only due to chaotic evolution of orbits. This is why we used

$$\begin{aligned}\delta f_\sigma &= (f_\sigma^{(2)} - f_\sigma^{(1)}) / f_\sigma^{(1)}, \\ \delta f_\varpi &= (f_\varpi^{(2)} - f_\varpi^{(1)}) / f_\varpi^{(1)}, \quad \text{and} \\ \delta f_\Omega &= (f_\Omega^{(2)} - f_\Omega^{(1)}) / f_\Omega^{(1)}\end{aligned}\quad (3)$$

as measures of chaotic diffusion in frequencies.

We have additionally attempted to reduce the effect of periodic oscillations of frequencies known as the problem of near harmonics (a consequence of a finite time window used for the Fourier transform—Nesvorný and Ferraz-Mello 1997a). We compute

$$\langle \delta f(a_k) \rangle_{2n+1} = \frac{1}{2n+1} \sum_{j=k-n}^{j=k+n} |\delta f(a_j)| - \frac{1}{2n+1} \left| \sum_{j=k-n}^{j=k+n} \delta f(a_j) \right|,\quad (4)$$

where $f(a_j)$ is a generic (resonant, perihelion, or nodal) frequency determined for the initial semi-major axis $a_j = 38.8 + 0.01j$, $0 \leq j \leq 101$. Assuming n initial conditions close to each other in the phase space, the problem of near harmonics makes the frequencies determined at these points oscillate with almost identical period and phase, so that if no chaotic evolution were present $\langle \delta f \rangle_n$ determined over these initial conditions (Eq. 4) vanishes. In the presence of chaotic diffusion, $\langle \delta f \rangle_n$ gives the net chaotic change. We plot $\langle \delta f_\sigma \rangle_5$, $\langle \delta f_\varpi \rangle_5$, and $\langle \delta f_\Omega \rangle_5$ for various eccentricities in Figs. 3d–3f. In the following text we refer to them simply as δf_σ , δf_ϖ , and δf_Ω , avoiding the use of $\langle \cdot \rangle_5$.

The color coding in Fig. 3 is similar to that in Fig. 2a: escaping and fast diffusing orbits with large changes of proper elements and frequencies are shown in yellow, light red represents the orbits with moderate chaotic diffusion, and blue represents the most stable orbits with negligible chaotic evolution.

In general terms, we note in Figs. 3a–3c that the chaotic evolution of A_σ (note the distinct color coding used in Fig. 3a) is more important than the chaotic evolutions of e and i (Duncan *et al.* 1995, Morbidelli 1997). For $e = 0.2$, the change of A_σ varies between 0.5° per 45 Myr in the center and 1° per 45 Myr in the immediate vicinity of unstable orbits on 10^8 years, while δe and δi range between 0.0003° and 0.003° and 0.1° and 0.5° per 45 Myr, respectively.

For the sake of a quantitative estimate of the diffusion effect over 4.5×10^9 years we may assume a random walk of orbital elements with a mean square displacement roughly proportional to time. Hence, δA_σ , δe , and δi over 4.5×10^9 years are expected to be some 10 times larger than the estimates over 4.5×10^7 years given in Figs. 3a–3c. This means that, for $e = 0.2$ and the trajectories within an interval of about 0.1 AU close to the strongly unstable region at large A_σ , the expected changes of δA_σ , δe , and δi over 4.5×10^9 years are roughly 10° , 0.03° , and 5° , respectively. While the changes in e and i are small to expect the trajectory to be destabilized in this way, the 10° change in A_σ is sufficient to insert many orbits initially at $115^\circ < A_\sigma < 125^\circ$ (for $e = 0.2$) into the strongly unstable region within the age of the Solar System. In Section 4, we give our definition of the marginally unstable region with respect to the number of bodies dynamically leaking from the resonance at 4×10^9 years after the initial instant.

For $e > 0.2$, δA_σ is generally larger or on the order of 1° per 45 Myr. The 4:1 and 5:1 three-body resonances are stronger for $e > 0.2$ and make A_σ change as much as a few degrees in 45 Myr at their locations. The 4:1 three-body resonance is located close to the unstable (yellow) region for $0.15 < e < 0.3$. This resonance enhances the chaotic diffusion making the marginally unstable region somewhat larger than it would be otherwise. The 5:1 three-body resonance is located at small amplitudes and the chaotic evolution of A_σ for $0.15 < e < 0.3$ at this resonance is confined by more regular behavior at both slightly larger and smaller A_σ than the resonant one ($\sim 60^\circ$ for $e = 0.2$). This more “regular” motion is not truly regular in the sense of a dense presence of KAM tori and an exponentially slow diffusion, but rather corresponds to trajectories with moderate chaotic changes

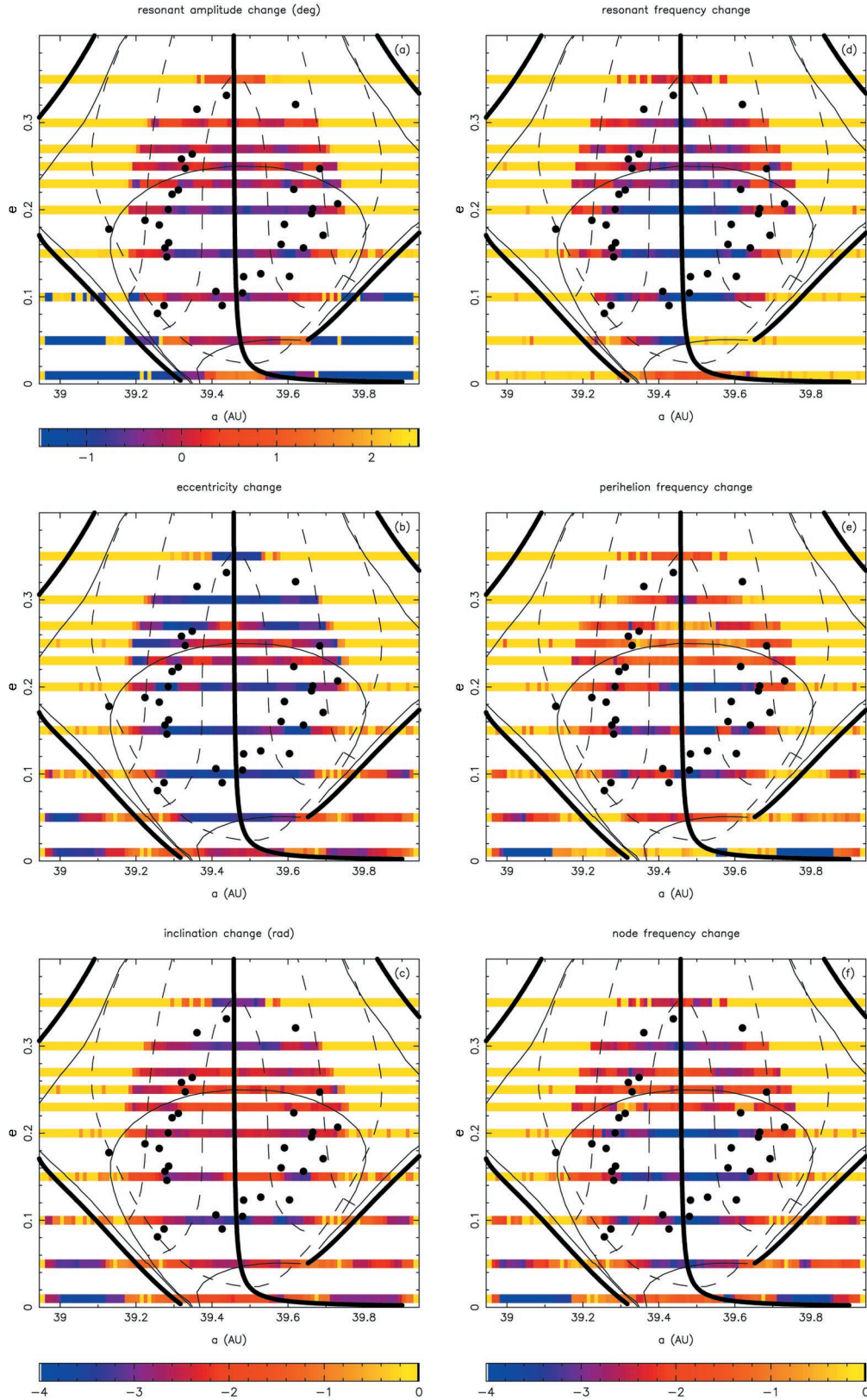


FIG. 3. Diffusion speed estimates in the 2:3 Neptune MMR. Variations of resonant amplitude (a), eccentricity (b), and inclination (c)— δi is given in radians—between two consecutive intervals of 45 Myr are shown (in logarithmic scale—note the distinct color coding of (a)). Smoothed relative changes of resonant (d), perihelion (e), and node frequencies (f) were computed for the same time interval. See text for the definition of these quantities.

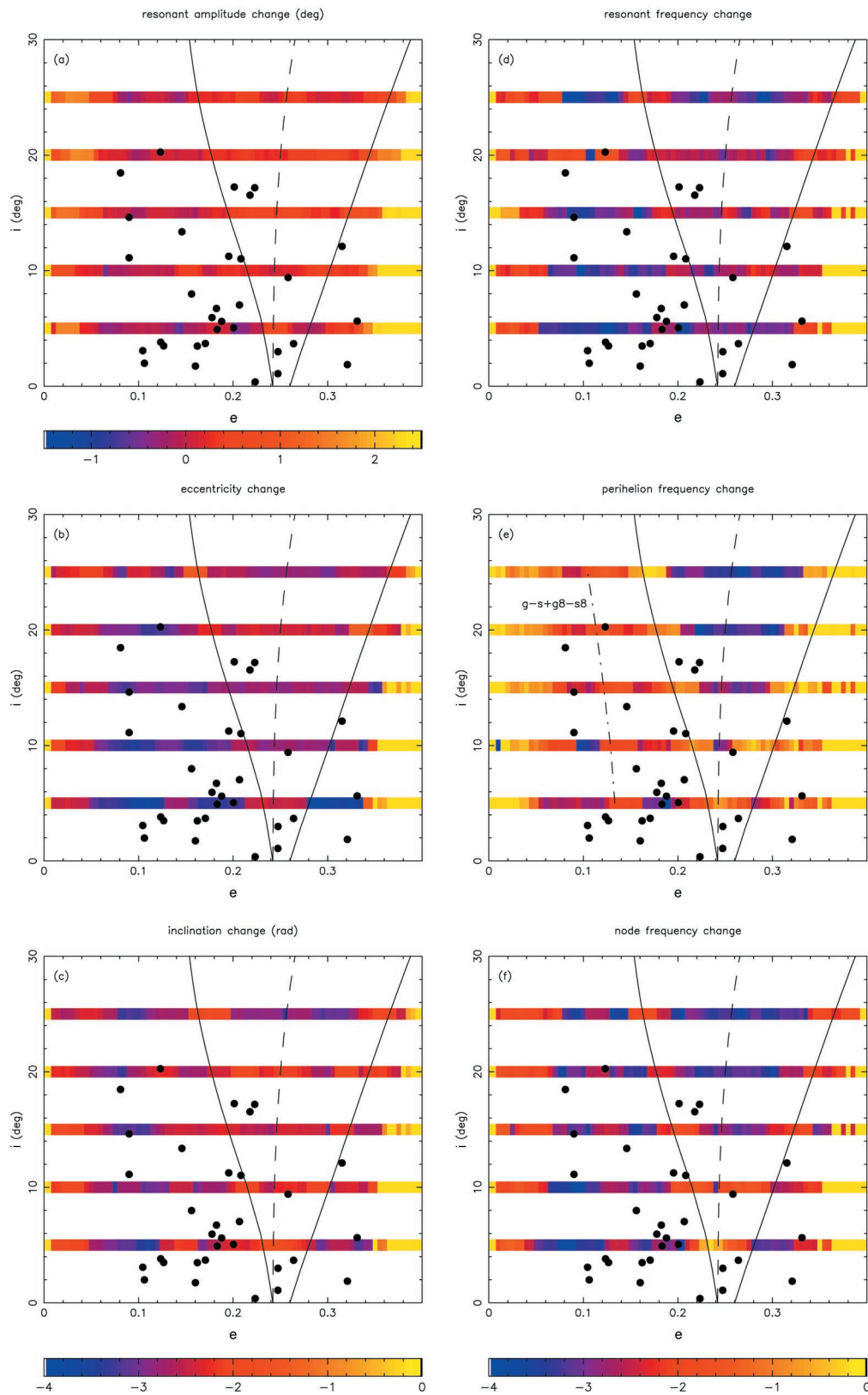


FIG. 9. Chaotic changes of the resonant amplitude (a), eccentricity (b), and inclination (c) on 45 Myr at $A_\sigma \sim 60^\circ$. Smoothed relative changes of the resonant (d), perihelion (e), and node frequencies (f) were computed on the same time interval. Note the enhanced values of δf at $e = 0.12$ – 0.14 due to the presence of the $g - s + g_8 - s_8$ secular resonance (dotted–dashed line in panel (e)).

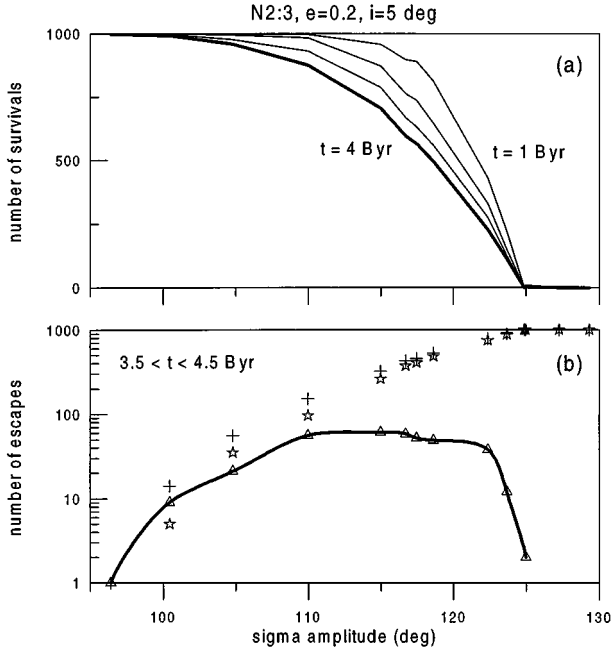


FIG. 4. (a) The number of particles surviving at $t = 1, 2, 3,$ and 4 Byr vs A_σ for initial $e = 0.2$. (b) Stars and crosses denote the numbers of escapes for $t < 3.5$ Byr and $t < 4.5$ Byr, respectively. Triangles denote their difference, i.e., escapes in $3.5 < t < 4.5$ Byr. The marginally unstable region is at $100^\circ < A_\sigma < 123^\circ$.

of orbital elements. Nevertheless, these trajectories form an effective barrier for the chaotic evolution of A_σ . Consequently, it is practically impossible that an orbit starting at the 5:1 three-body resonance and $0.15 < e < 0.3$ escapes from the 2:3 Neptune MMR within 4×10^9 years.

Several other conclusions can be inferred from Figs. 3a–3c:

(1) The most regular space of the 2:3 Neptune MMR at low inclinations is at $0.1 < e < 0.2$ and small to moderate A_σ , where $\delta A_\sigma \lesssim 0.5^\circ$ per 45 Myr. There is an area in the middle of the above interval ($e = 0.15$) where $\delta i = 0.8^\circ$ per 45 Myr. We show later that this happens due to the presence of a secular resonance involving the argument of perihelion (Fig. 9e).

(2) δe and δi are enhanced at the Kozai resonance ($0.22 < e < 0.27$). Typically, $0.0006 < \delta e < 0.006$ per 45 Myr and $0.1 < \delta i < 0.6^\circ$ per 45 Myr. While the eccentricity evolution is confined within the interval $0.22 < e < 0.27$ and no macroscopic changes of e are to be expected (if the inclination stays low), the inclination can chaotically evolve by several degrees in 4×10^9 years along the separatrices of the Kozai resonance (Section 5). This evolution, however, never leads to escapes providing the initial inclination is small ($i \lesssim 10^\circ$).

(3) The test particles starting near the separatrices of the 2:3 MMR and with $e < 0.1$ usually spend a time period exceeding 10^8 years with σ alternating between libration and circulation. At these eccentricities, orbits are well separated from Neptune and the chaotic region at the borders of the 2:3 MMR is confined from both sides in a , which does not permit a definitive escape

from the resonance through an increase of A_σ . On the other hand, the chaotic evolution of e (and i) is fast near separatrices, where $\delta e > 0.05$ ($\delta i > 5^\circ$) per 45 Myr; so that in several 10^8 years, the test particles are transferred to $e \sim 0.2$, where they encounter Neptune and leave the resonance.

(4) On both sides of the 2:3 MMR ($a = 39.05$ and 39.8 AU), there are places of stable motion at $e < 0.1$. Note that δA_σ and δf_σ are fake here because the motion is non resonant, but other indicators are correct. Both places are unpopulated.

The relative changes in frequencies (Figs. 3d and 3e) are complementary to action changes. δf_σ , δf_ω , and δf_Ω should be regarded as more precise measures of chaotic diffusion than δA_σ , δe , and δi , because of the nature of frequency analysis. On the other hand, frequency changes are harder to interpret because they do not measure the diffusion rate in the “direction” of orbital elements, so that modifications of orbits are represented indirectly by them.

δf_σ measures the local chaotic evolution in the plane transversal to the lines of $f_\sigma = \text{const}$. The lines of the 4:1 and 5:1 three-body resonances correspond to $f_\sigma = 5.91 \times 10^{-5} \text{ year}^{-1}$ and $f_\sigma = 4.73 \times 10^{-5} \text{ year}^{-1}$, so that roughly $\delta f_\sigma = 0.22$ is needed to transit between them. This is apparently beyond the possibilities of chaotic orbital evolution because $\delta f_\sigma = 10^{-4} - 10^{-3}$ per 45 Myr, i.e., $\delta f_\sigma = 10^{-3} - 10^{-2}$ per 4.5 Byr, in the region between these three-body resonances (Fig. 3d). Hence, this verifies the stability of the central region of the 2:3 Neptune MMR.

4. THE marginally UNSTABLE REGION

The chaotic diffusion in the 2:3 Neptune MMR is dominated by the evolution in A_σ . This simplifies the situation and allows us to model chaotic diffusion as a one-dimensional random walk.

We started 1000 test particles at the same initial value A_σ^0 . For each particle, a random walk was simulated according to the size of δA_σ (Fig. 3a). In short, for a given instantaneous A_σ^n obtained at the step n of the algorithm, we determined the value of $\delta A_\sigma(A_\sigma^n)$ (interpolating from the archive of δA_σ vs A_σ previously computed for all 101 test particles at given value of e —Section 3.2) and then randomly added or subtracted this quantity from A_σ^n , so that $A_\sigma^{n+1} = A_\sigma^n \pm \delta A_\sigma(A_\sigma^n)$. The same procedure was repeated in the next step with A_σ^{n+1} .

We ran this simulation for 4.5×10^9 years. The particles that had $A_\sigma^n > 170^\circ$ for some n were judged to escape from the resonance and were deleted from the simulation. The final result was the ratio of the number of the deactivated test particles to that of survived particles. We sampled the resonant amplitudes repeating the above procedure with initial A_σ^0 uniformly spaced between 0 and 170° . Hence, for given e , we ended up with the number of escapes/survivals at time t ($0 < t < 4.5$ Byr) as a function of A_σ^0 .

Figure 4a shows the number of surviving particles at 1, 2, 3, and 4 Byr for $e = 0.2$. All particles with $A_\sigma^0 < 95^\circ$ survive while those with $A_\sigma^0 > 125^\circ$ escape. For intermediate amplitudes the number of survivals smoothly decreases with A_σ^0 . The profile

is less steep for $t = 4$ Byr than for $t = 1$ Byr corresponding to the fact that test particles with initially smaller A_σ escape on longer time intervals. The profile at $t = 4$ Byr should roughly correspond to the current density of the 2:3 resonant objects at intermediate amplitudes. However, it is too early to draw conclusions about whether this profile represents well the real 2:3 MMR population, because too few Plutinos are presently known.

Figure 4b shows the number of test particles escaping for $t < 4.5$ Byr (crosses) and $t < 3.5$ Byr (stars) for $e = 0.2$. It also shows their difference, which is the number of particles escaping in $3.5 < t < 4.5$ Byr (triangles). This last quantity approximates the current escape rate from the 2:3 MMR. The test particles giving a contribution larger than 1% start at $101^\circ < A_\sigma < 124^\circ$.

We define a place in the phase space to be *marginally unstable* if the escape rate to Neptune crossing orbits at $t = 4$ Byr is more than 1% of the initial population per 1 Byr.² The places for which the escape rate at $t = 4$ Byr is less than 1% are: (i) strongly unstable, where most of the original population escapes at $t < 4$ Byr so at $t = 4$ Byr there are too few surviving bodies, and (ii) practically stable, where the mean lifetime of bodies is much longer than the age of the Solar System and the escape rate at $t = 4$ Byr is also negligible. For practical reasons, we assume the escape rate at $t = 4$ Byr to be equal to the relative number of escapes between 3.5 and 4.5 Byr and identify the marginally unstable region as the interval of A_σ in which more than 1% of the original population leaks from the resonance in $3.5 < t < 4.5$ Byr.

Figure 5 shows how the width of the marginally unstable region depends on e . For $0.05 < e < 0.35$, we show the number of escapes at $3.5 < t < 4.5$ Byr (triangles) and trace the left and right borders of the marginally unstable region, where the number of escapes was larger than 10 (from initial 1000 test particles—i.e., larger than 1%), by spline smoothing (dotted lines).

The size of the marginally unstable region does not change much for $0.1 < e < 0.27$ and accounts for 20° – 30° centered at $A_\sigma \sim 110^\circ$. This roughly corresponds to the area affected by the 4:1 three-body resonance (Figs. 2 and 3). Duncan *et al.* (1995) found that the resonant bodies are unstable on billion year time scales if initially $70^\circ < A_\sigma < 130^\circ$. From Fig. 5, we would rather say that the lower limit of this range is 90° – 100° for a wide range in e , and resonant KBOs with $70^\circ < A_\sigma < 90^\circ$ are perfectly stable.

For $e = 0.3$, the marginally unstable region extends from about 55° to 105° and occupies more than half of the resonant space. According to Fig. 3a, the diffusion in A_σ is faster at $e = 0.3$ than at smaller e , allowing for larger mobility of test particles.

For $e = 0.35$, the marginally unstable amplitudes are those between 0° and 40° . Here however, the model of one-dimensional random walk in A_σ might not be realistic because a small change in e (instead of A_σ) can destabilize orbits. Note that the number of late escapes at this e is large ($\sim 20\%$) suggesting a large con-

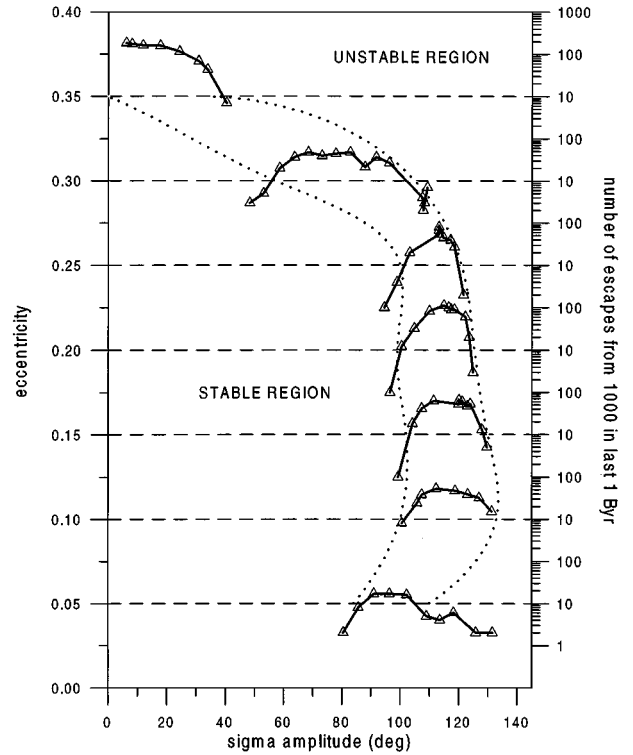


FIG. 5. The position and width of the marginally unstable region in dependence on e . We compute the marginally unstable region as the place where more than 1% of the initial population escapes in $3.5 < t < 4.5$ Byr. This percentage corresponds in our experiment to more than 10 escapes (from 1000)—dashed horizontal lines. The dotted lines show the boundaries of the marginally unstable region.

tribution to the currently escaping objects from the 2:3 MMR. However, primordial orbits at $e = 0.35$ would have been rare.

The one-dimensional random walk model is incomplete also for $e \sim 0.05$. There the test particles must first chaotically evolve to larger e before they can leave the resonance by close encounters with Neptune. This evolution can be slow and 10^8 – 10^9 years may pass before a particle definitely leaves the resonance. For this reason, the limits of the marginally unstable region at $e = 0.05$ shown in Fig. 5 are only approximate. On the other hand, no Plutinos are observed at these eccentricities so that the contribution of objects initially at $e \sim 0.05$ to the total present flux of the escaping bodies from the 2:3 MMR is small.

5. AN ESTIMATE OF THE RESONANT POPULATION

We proceed with the calculation of ratios between the numbers of primordial, current, and escaping (in the last 1 Byr) bodies. Let us suppose that the angles of 2:3 resonant bodies and their semi-major axes were initially uniform. We show later that this assumption is not in contradiction to the scenario in which the 2:3 MMR objects were captured by resonance sweeping (Malhotra 1995). Moreover, we suppose that the inclinations were not excessively large, so that the diffusion speed measured at $i = 5^\circ$ is representative (observed Plutinos have on average $i = 9.3^\circ$).

² If $P(t)$ is the percentage of test particles escaping from the initial population in the time interval $[0, t]$, then by the escape rate at time t we mean the derivative of this function.

The number of primordial objects with orbits within 1° around given A_σ is proportional to the volume in the phase space occupied by such orbits: $\Delta V(A_\sigma)$. In the averaged, planar, circular model of the 2:3 MMR, with Neptune as the only perturbing body, this volume can be easily determined. The above model is integrable and the trajectories in a, σ are computed on manifolds of the motion integral $N = \sqrt{a}(-2/3 + \sqrt{1-e^2})$. The area $V(A_\sigma)$ enclosed by a trajectory is computed as

$$V(A_\sigma) = \int_0^{T_\sigma} (a(t) - a_{\text{res}}) \dot{\sigma} dt, \quad (5)$$

where $\dot{\sigma}$ is the time derivative of σ and the integral is evaluated over one period of σ . The derivative of $V(A_\sigma)$ with respect to A_σ times 1° is the needed volume $\Delta V(A_\sigma)$. This volume grows with A_σ , which means that the orbits with initially large A_σ were more common. For instance, the volume occupied by orbits at $A_\sigma = 85^\circ$ is a factor of 10 larger than the volume occupied by orbits at $A_\sigma = 10^\circ$. This implies that the primordial orbits at $A_\sigma \sim 110^\circ$, i.e., in the marginally unstable region, were by a factor of 10 more numerous than the primordial stable orbits with small A_σ .

In Fig. 6a, the dashed line shows the initial distribution in A_σ resulting from a uniform initial distribution in orbital angles and a . Comparing this distribution with the one that would have re-

sulted from the capture by resonance sweeping (Malhotra 1997, her Fig. 4), we find no difference for $0^\circ < A_\sigma < 90^\circ$, where the captured population is exactly proportional to the volume. Consequently, the non-uniformity of Malhotra's captured population in this range of A_σ is not a result of some special process involved in the resonant capture, but rather reflects the uniform distribution in a and orbital angles. The captured population is peaked at moderate amplitudes due to the dynamic instability at large A_σ . The position of this peak in A_σ depends on the eccentricities of the pre-capture objects and the rate at which the resonances sweep through the primordial KB. It can be expected that small pre-capture e and even a slow sweeping rate would result in a resonant distribution peaked at small A_σ , while larger e and faster sweeping would lead to a post-capture population that covers the stable resonant space more uniformly (i.e., following the dashed line in Fig. 6a). In the example given by Malhotra (1997), the resonant population is peaked at 90° and it is in fact very close to the uniform coverage of the 2:3 Neptune MMR eroded at large A_σ over several 10^7 years, which was the time used in the capture simulation. For this reason, our assumption of initially uniform semi-major axes and angles approximately holds for the resonance sweeping scenario.

We assume a primordial population of N_{prim} bodies uniformly distributed in a, λ, ω , and Ω (not in A_σ), initially located at the same e in the stable and marginally unstable regions with $A_\sigma < A_\sigma^*$ (A_σ^* is the outer border of the marginally unstable region—for $e = 0.2$, $A_\sigma^* = 127^\circ$). Then, we compute for each A_σ ,

$$N_{\text{esc}}(A_\sigma, e) = N_{\text{prim}} \times \frac{\Delta V(A_\sigma, e)}{V(A_\sigma^*(e))} \times f_{\text{esc}}(A_\sigma, e), \quad (6)$$

where $f_{\text{esc}}(A_\sigma, e)$ is the percentage of objects with initial e escaping from initial A_σ in the last 1 Byr (Fig. 5). $N_{\text{esc}}(A_\sigma, e)$ is the number of objects with initial e having the initial resonant amplitude within 1° of A_σ and escaping in the last 1 Byr. The integral of the above expression over the amplitudes $0 < A_\sigma < A_\sigma^*$ gives $N_{\text{esc}}(e)$, which is the total number of escaping objects with initial e in the last 1 Byr. For $e = 0.2$, the total area enclosed by the trajectory with A_σ^* is $V(A_\sigma^*(e)) = 116.6 \text{ AU} \times \text{deg}$, and $N_{\text{esc}}(e)/N_{\text{prim}} = 0.0165$, i.e., some 1.7% of the objects initially present at $e = 0.2$ in the 2:3 MMR escape in the last 1 Byr. We have calculated the same ratio also for $e = 0.1$ and $e = 0.3$ (Table I).

Integrating $N_{\text{esc}}(e)/N_{\text{prim}}$ over e allows us to determine the total fraction of objects escaping per 1 Byr from the 2:3 Neptune MMR at $t = 4$ Byr. From Table I, and assuming an initially uniform distribution of e in the interval $0.1 < e < 0.3$, this fraction results in 1.2% bodies per 1 Byr. Moreover, using the results of Section 4 (e.g., Fig. 4a) together with a relation similar to that of Eq. (6), it is also possible to determine the fraction $N_{\text{surv}}(e)/N_{\text{prim}}$ of objects that survive at $t = 4$ Byr (Table I). Integrating this fraction over e we obtain that 70% of objects survive in the 2:3 MMR at $t = 4$ Byr. Below, we calibrate these

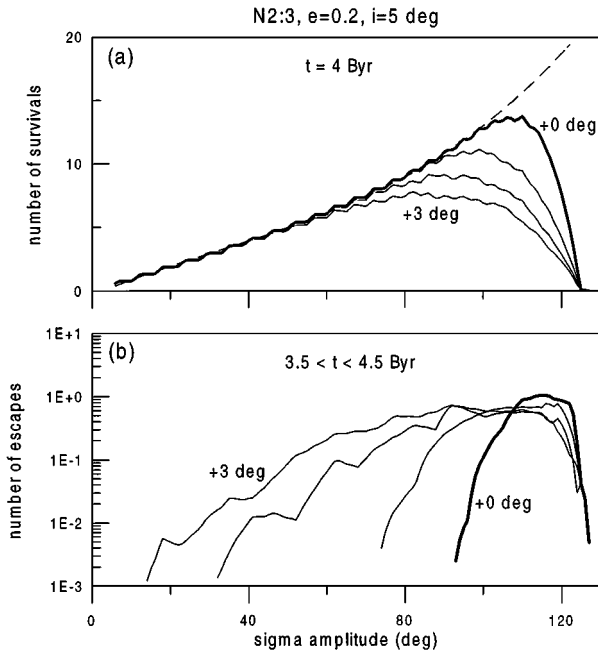


FIG. 6. The number of test particles surviving at $t = 4$ Byr (a), and the number of escapes in $3.5 < t < 4.5$ Byr (b), as a function of A_σ . The dashed line in (a) shows the density (per 1°) of the original population of 1000 test particles. The bold line denoted $+0^\circ$ shows how the population is eroded at $t = 4$ Byr under the effect of slow chaotic diffusion driven by four outer planets ($\delta A_\sigma^{\text{diff}}$). The erosion is larger for $\delta A_\sigma^{\text{kick}} = 1^\circ, 2^\circ$, and 3° , the latter being denoted by $+3^\circ$. Note in (b) how the active region, where objects escape in $3.5 < t < 4.5$ Byr, enlarges with increasing contribution of the collision/scattering kicks.

TABLE I
The Statistics of Surviving and Escaping Populations
in the 2:3 Neptune MMR

e	A_σ^* (deg)	$V(A_\sigma^*)$ (AU \times deg)	$N_{\text{esc}}/N_{\text{prim}}$	$N_{\text{surv}}/N_{\text{prim}}$	$N_{\text{esc}}/N_{\text{surv}}$
0.1	135	107.4 (92.1%)	0.00937 (52.3%)	0.827 (94%)	0.0113 (51.3%)
0.2	127	116.6 (100%)	0.0165 (100%)	0.810 (100%)	0.0203 (100%)
0.3	112	89.3 (76.6%)	0.0121 (56.0%)	0.563 (53.3%)	0.0215 (81.1%)

Note. The individual columns are eccentricity (e), amplitude limiting the stable and marginally unstable regions (A_σ^*), area enclosed by the curve with amplitude A_σ^* ($V(A_\sigma^*)$), and ratios $N_{\text{esc}}/N_{\text{prim}}$, $N_{\text{surv}}/N_{\text{prim}}$, and $N_{\text{esc}}/N_{\text{surv}}$, where N_{surv} is the number of bodies surviving at $t = 4$ Byr (determined from Eq. (6), with $f_{\text{surv}}(A_\sigma)$ for $e = 0.2$ shown in Fig. 4a). The percentages in brackets are the relative contributions of $e = 0.1$ and $e = 0.3$ with respect to $e = 0.2$.

numbers by the number of bodies needed to keep the observed population of the Jupiter–family comets (JFC) in steady state.

According to Levison and Duncan (1997), the total number of visible ($q = a(1 - e) < 2.5$ AU) active and extinct JFCs with $H_T < 9$ (H_T is the total magnitude of an active comet³) is about 500. The main uncertainty in this estimate comes from the necessity to compute the ratio between the numbers of extinct and active JFCs: Levison and Duncan (1997) adopted a physical lifetime of an active comet to be 12,000 years, and determined the above ratio to be 3.5. Moreover, Levison *et al.* (2000) estimated the ratio between the JFCs and the ecliptic comets (ECs) (i.e., comets having their Tisserand parameters larger than 2 unless they are on stable orbits in the trans-Neptunian region). Then, they computed the current number of the ECs to be $N_{\text{EC}} = 1.3 \times 10^7$ and also determined their mean dynamic lifetime: $t_{\text{EC}} = 1.9 \times 10^8$ yr.

The EC may be resupplied from the classical KB ($35 < a < 50$ AU, moderate e) or may be a remnant of the massive Scattered Disk (SD; Duncan and Levison 1997). Denote by $f_{2:3/\text{all}}$ the ratio of the number of comets escaping from the 2:3 MMR to the total contribution of the classical KB and SD. If, for instance, most comets come from the classical KB (including the 2:3 Neptune MMR) and the contribution of the SD is negligible, then it would be reasonable to assume that $f_{2:3/\text{all}} \sim 0.1$ – 0.2 . Indeed, the current population of the 2:3 Neptune MMR is estimated to be between 10 and 20% of the classical KB population (Jewitt *et al.* 1998).

The current number of objects in the 2:3 Neptune MMR (N_{surv}) corresponding to $H_T < 9$ can be computed from

$$N_{\text{surv}} r_{2:3} = f_{2:3/\text{all}} \frac{N_{\text{EC}}}{t_{\text{EC}}}, \quad (7)$$

³ It is unclear how to relate the absolute magnitude of an active comet to the diameter of its nucleus. According to Levison *et al.* (2000) and references therein, the absolute magnitudes $H_T < 9$ should roughly correspond to diameters $D > 1$ – 3 km.

where $r_{2:3} = N_{\text{esc}}/N_{\text{surv}}$ is the relative fraction of the present resonant population that escapes from the 2:3 MMR per time interval. From previously determined $N_{\text{esc}}/N_{\text{prim}}$ and $N_{\text{surv}}/N_{\text{prim}}$, $r_{2:3} = 1.7 \times 10^{-11} \text{ year}^{-1}$. This number is smaller than $r_{\text{KB}} = 3$ – $4 \times 10^{-11} \text{ year}^{-1}$ determined by Duncan *et al.* (1995) for the whole classical KB (including the 2:3 Neptune MMR). Substituting $r_{2:3}$, N_{EC} , and t_{EC} in Eq. (7), $N_{\text{surv}} = 4 \times 10^9 f_{2:3/\text{all}}$. Assuming $f_{2:3/\text{all}} = 0.15$ we conclude that there are currently 6×10^8 objects with $H_T < 9$ in the 2:3 Neptune MMR.

This number is about the same as the 4.5×10^8 comets estimated by Morbidelli (1997). There are several differences between this and Morbidelli’s work: (1) Morbidelli estimated that the volume of the region where bodies are either on invariant tori or having orbits with diffusion speed too slow to escape from the 2:3 MMR over the age of the Solar System is about 40% of the volume of the moderately slow diffusion region. In this work we estimate the volume of the stable region to be about 80% of the volume of the marginally unstable region. (2) Morbidelli assumed that $f_{2:3/\text{all}} = 0.25$, while $f_{2:3/\text{all}} = 0.15$ in our estimate. (3) The initial conditions with small A_σ were almost absent in Morbidelli’s work. This can be presumably due to the choice of $a = 39.5$ AU in his experiment, which is not necessarily the semi-major axis corresponding to $A_\sigma \sim 0$ because of the short-periodic variations induced by Jupiter. (4) While $N_{\text{esc}}/N_{\text{surv}} = 0.11$ in Morbidelli (1997), in this paper $N_{\text{esc}}/N_{\text{surv}} = 0.017$. (5) Morbidelli’s calibration used estimates of Duncan *et al.* (1995) who found that the needed flux to sustain the JFC is 0.21 comets/year, while this work uses $N_{\text{EC}}/t_{\text{EC}} = 0.068$ comets/yr from Levison *et al.* (2000). In view of the above differences, the agreement between our $N_{\text{surv}} = 6 \times 10^8$ and Morbidelli’s $N_{\text{now}} = 4.5 \times 10^8$ is rather surprising.

6. A SIMPLE MODEL OF COLLISIONS/SCATTERING

Until now, we did not address other possible mechanisms by which the 2:3 resonant objects could be destabilized: (i) collisional fragmentation, (ii) collisional non-disruptive kicks, (iii) mutual dynamical scattering at close encounters, or (iv) the dynamical scattering by Pluto. Detailed analysis of the effect of these processes goes beyond the scope of this paper, but we have attempted to simulate them by a simple scheme, adding to $\delta A_\sigma^{\text{diff}}$ (i.e., the change in A_σ due to the dynamic chaotic diffusion, Eq. 2) an arbitrary quantity $\delta A_\sigma^{\text{kick}}$ assumed to come from the random kicks generated by the above processes. Not knowing the dependence of $\delta A_\sigma^{\text{kick}}$ on e , i , and A_σ (and time), we have assumed $\delta A_\sigma^{\text{kick}}$ to be constant.

Farinella *et al.* (2000) estimated that the population of KBOs larger than about 100 km in diameter has not been significantly altered by collisions over the age of the Solar System. This means that collisional fragmentation is not relevant for large bodies. Conversely, this mechanism may be dominant for small bodies since about 10 fragments, 1 to 10 km in size, are currently produced per year in the KB at 40 AU (Farinella *et al.* 2000). With ejection speeds of 10–100 m/s, these fragments have

semi-major axes about 0.1–1 AU different from those of their parent bodies.

Levison and Stern (1995) investigated the effect of collisional and scattering kicks on Pluto and found that the gravitational scattering by 1–330 km objects is much more important than physical collisions. From their Fig. 8 we can infer that $\delta A_\sigma^{\text{scat}}$ is on the order of 10° per 5×10^7 years, but this assumes a dense primordial population of 2.7×10^7 comets per AU^2 near 40 AU, which is more than a factor of 100 larger than the current population of the KBOs at 40 AU. If $\delta A_\sigma^{\text{scat}}$ scales linearly with the number of objects, then this indicates that the current $\delta A_\sigma^{\text{scat}}$ of Pluto should be on the order of 0.1° per 5×10^7 years. Recall that smaller bodies must be scattered more than Pluto.

Nesvorný *et al.* (2000) calculated the random walk of Plutinos driven by the gravitational scattering by Pluto. While for $i < 5^\circ$, $\delta A_\sigma^{\text{Pluto}}$ is on the order of 1° per 45 Myr, for $i > 10^\circ$ $\delta A_\sigma^{\text{Pluto}} = 2^\circ$ – 6° per 45 Myr, depending on the eccentricity.

Figure 6 shows the results of random walks characterized by $\delta A_\sigma^{\text{diff}} + \delta A_\sigma^{\text{kick}}$, where we choose different values of $\delta A_\sigma^{\text{kick}}$. The scale on the y-axis corresponds to 1000 test particles at $e = 0.2$, initially distributed between 0 and A_σ^* according to the area occupied by the orbits with given A_σ (dashed line in Fig. 6a). This scale gives the number of particles per 1° . In Fig. 6a, we show the number of surviving test particles at $t = 4$ Byr and in Fig. 6b we show the number of particles escaping in $3.5 < t < 4.5$ Byr. Bold lines (denoted by +0) are the results of purely dynamic random walk with no contribution of kicks. Thin lines show the results for $\delta A_\sigma^{\text{kick}} = 1^\circ, 2^\circ$, and 3° per 45 Myr, respectively (the last one being denoted by +3). Table II summarizes the statistics of surviving and escaping particles in each case.

The current density of objects in the 2:3 MMR should roughly correspond to one of the curves in Fig. 6a. The erosion at large A_σ increases with the increasing role of random kicks. The density peak shifts from $A_\sigma = 105^\circ$, when the evolution is dominated by pure dynamic chaotic diffusion, to $A_\sigma = 85^\circ$, when $\delta A_\sigma^{\text{kick}} = 3^\circ$. Moreover, for $\delta A_\sigma^{\text{kick}} = 3^\circ$ the density curve is much flatter than that for $\delta A_\sigma^{\text{kick}} = 0^\circ$. The values of $N_{\text{surv}}/N_{\text{prim}}$ in Table II show that the primordial population of the 2:3 MMR is reduced to 56% for $\delta A_\sigma^{\text{kick}} = 3^\circ$ and only to 81% for $\delta A_\sigma^{\text{kick}} = 0$. We believe that with increasing knowledge of the orbital distribution of Plutinos, one should be able to estimate the contribution

TABLE II

The Statistics of the Primordial, Surviving, and Escaping Populations at $e = 0.2$ for Different Contributions of Random Kicks Generated by Collisions, Mutual Scattering, and Scattering by Pluto

$\delta A_\sigma^{\text{diff}} + \delta A_\sigma^{\text{kick}}$	$N_{\text{esc}}/N_{\text{prim}}$ (%)	$N_{\text{surv}}/N_{\text{prim}}$ (%)	$N_{\text{esc}}/N_{\text{surv}}$ (%)
δA_σ	1.65	81.1	2.03
$\delta A_\sigma + 1^\circ$	1.99	71.4	2.78
$\delta A_\sigma + 2^\circ$	2.45	63.3	3.87
$\delta A_\sigma + 3^\circ$	3.06	56.3	5.44

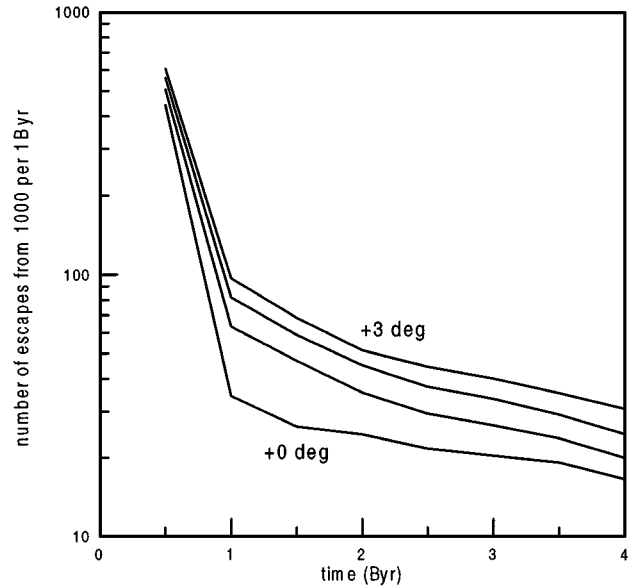


FIG. 7. The number of escapes per 1 Byr is shown as a function of time for $\delta A_\sigma^{\text{kick}} = 0^\circ, 1^\circ, 2^\circ$, and 3° . The original population accounted for 1000 test particles at $e = 0.2$, distributed between $0 < A_\sigma < A_\sigma^*$ following the dashed line in Fig. 6a.

of collisions/scattering to the general random walk in the 2:3 Neptune MMR on the basis of the comparison with Fig. 6a.

Figure 6b shows how the marginally unstable region enlarges with the increasing role of collisions/scattering. For $\delta A_\sigma^{\text{kick}} = 3^\circ$, $N_{\text{esc}}/N_{\text{surv}} = 3.1\%$ —almost double the 1.7% determined from the dynamic chaotic diffusion alone. If the former percentage were true, the present number of objects in the 2:3 MMR with $H_T < 9$ would be estimated to be about 3×10^8 (assuming $f_{2:3/\text{all}} = 0.15$). Of course the above model is a very rough approximation of the real collisional dynamics in the 2:3 MMR because it does not account for the disruption of bodies and does not allow for the resulting changes in the size distribution of objects.

In Fig. 7, we show the number of escapes per 1 Byr (scaled to the primordial population of 1000 test particles at $A_\sigma < A_\sigma^* = 127^\circ$ for $e = 0.2$) from the 2:3 MMR as a function of time. As expected, most escaping particles leave the resonance at $t < 1$ Byr. If the 2:3 MMR is the sole source of bodies crossing outer planets' orbits, then the cratering record on planetary satellites should have a time dependence similar to that of the curves in Fig. 7. A steeper cratering rate in the last 3 Byr would indicate a significant role of collisions and/or scattering in the source region.

7. THE RUN FOR LARGER INCLINATIONS

The estimate of the maximum LCE at $t = 10^8$ years is plotted in Fig. 8a as a function of initial e and i , and for the second set of initial conditions (Section 2). The initial a was 39.41 AU, which means that the test particles started with $A_\sigma = 60^\circ$, i.e., with A_σ only slightly smaller than most observed 2:3 resonant objects.

The libration centers (dashed line) and separatrices (full lines) of the Kozai resonance were computed for $A_\sigma = 0$ by a semi-numerical method. The minimum distances of test particles to Neptune in 10^8 years are shown in Fig. 8b. The color coding is the same as in Fig. 2. The eccentricity and inclination of Pluto (\oplus) and known Plutinos (large dots) are shown at the intersection of their trajectories with $\sigma = 180^\circ$ and $\omega = 90^\circ$ (from Nesvorný *et al.* 2000).

The central, weakly chaotic region of the 2:3 MMR extends to high inclinations (Fig. 8a). While the convergence of $\ln \Delta(t)/t$ to an asymptotic non-zero value ($\sim 10^{-6.5} - 10^{-7}$ year $^{-1}$) is evident for all trajectories in the Kozai resonance, we have LCE $\leq 10^{-7}$ yr $^{-1}$ at $e = 0.1$. The chaotic region at small e , where LCE $\sim 10^{-5} - 10^{-5.5}$ yr $^{-1}$, slightly enlarges with increasing i (from $e < 0.05$ at $i = 5^\circ$ to $e < 0.07$ at $i = 25^\circ$). This chaos is almost certainly due to the overlap of the 2:1, 3:1, and 4:1 secondary resonances, because the ν_{18} secular resonance is limited to $i < 10^\circ$ and has a large libration period. The region of escapes at $e > 0.35$ for $i = 5^\circ$ shifts to larger e with increasing i . This is either due to the changing positions and sizes of the ν_8 and ν_{18} secular resonances or because the orbits with large inclinations are better separated from Uranus. The minimum distance of test particles to Neptune decreases from ~ 20 AU in the center of the Kozai resonance to ~ 15 AU just outside its left limit and further to ~ 10 AU at $e \sim 0$.

Figure 9 shows the chaotic change of orbital elements and frequencies in 45 Myr. The computational procedure was exactly the same as that in Section 3.2 (Eqs. 2–4).

The dependence of δA_σ (Fig. 9a) on the initial orbital elements has characteristics similar to those of the LCE (Fig. 8a). δA_σ is large for $e < 0.05$ ($\sim 20^\circ - 30^\circ$ per 45 Myr) showing the instability of the corresponding orbits. These orbits evolve to the separatrices of the 2:3 MMR in several 10^8 year. Such evolution is accompanied by a random walk in e (and i), which gets faster near separatrices, where $\delta e > 0.05$ ($\delta i > 5^\circ$) per 45 Myr (Figs. 3b and 3c).

δA_σ is moderately larger in the Kozai resonance ($2^\circ - 4^\circ$ per 45 Myr) than in the rest of the resonant space ($\sim 1^\circ$ per 45 Myr at $e = 0.1$). This can also be an effect of the 5:1 three-body resonance located at $A_\sigma \sim 60^\circ$, where our initial conditions cross the resonant space.

The e and i evolutions (Figs. 9b and 9c) are moderately enhanced at the separatrices of the Kozai resonance ($\delta e \sim \delta i \geq 10^{-2.5}$). The orbits starting with large A_ω significantly evolve in e and i on billion year time scales. At $i > 10^\circ$, the right separatrix of the Kozai resonance is separated only by 0.03–0.04 in e from the high- e unstable region. As the expected chaotic evolution of e on 4×10^9 years is of this size, most of the initially large- A_ω orbits with $i > 10^\circ$ are unstable. These findings are in agreement with the results of Levison and Stern (1995) concerning the stability at Pluto-like inclinations. The two Plutinos residing just outside the right separatrix of the Kozai resonance at $e = 0.32 - 0.33$ and $i \leq 5^\circ$ occupy a space where the evolution in e is moderate.

The stability of small- A_ω orbits in the Kozai resonance is evident on the evolution of frequencies. For $i > 10^\circ$, $\delta f_\varpi \sim 10^{-3}$ on 45 Myr (Fig. 9e), which means only a 1% change in 4.5 Byr. For $i = 15^\circ$ and $A_\sigma = 60^\circ$, the stable motion in the Kozai resonance extends at $0.22 < e < 0.29$, which roughly corresponds to $A_\omega < 50^\circ$. For larger initial A_ω , f_ϖ significantly evolves and at the separatrices of the Kozai resonance δf_ϖ is as large as 10% over the age of the Solar System.

Although our initial conditions do not cover the region at $i > 25^\circ$, it is very likely that the stable motion in the center of the Kozai resonance extends to higher inclinations. In such a case, the result of Duncan *et al.* (1995) that the MMRs with Neptune have a destabilizing effect for $i \geq 25^\circ$ is only approximate. Indeed, the initial conditions of high- i simulations of Duncan *et al.* sampled orbits with $e \leq 0.1$, which according to Fig. 9 are more easily destabilized by secular effects.

Note in Fig. 9e the slightly anomalous value of δf_ϖ at the dotted-dashed line. We have identified it to be the secular resonance with angle $\omega + \varpi_N - \Omega_N$. Figure 10 shows the evolution of this resonant angle for the test particle started at $a = 39.41$ AU, $e = 0.135$, and $i = 15^\circ$. This secular resonance is usually denoted by $g - s + g_8 - s_8$, where $g = f_\varpi$, $s = f_\Omega$, and $g_8 = 0.6727''/\text{year}$ and $s_8 = -0.6914''/\text{year}$ are Neptune's perihelion and nodal mean frequencies. We have plotted its position in Fig. 9e from $f_\varpi(e, i)$ and $f_\Omega(e, i)$ calculated by frequency analysis. For $i \leq 15^\circ$, this resonance does not provide an escaping route from the 2:3 MMR because it is confined from both sides in e by more regular motion. For larger inclinations, transitions to separatrices of the Kozai resonance and to the low- e unstable region are possible. The $g - s + g_8 - s_8$ secular resonance does not appear in the plot of the LCE because of the large period of its resonant angle.

8. THE DISTRIBUTION OF RESONANT OBJECTS

From 191 KBOs currently registered in the Asteroid Orbital Elements Database of Lowell Observatory (September 1999), 68 objects fall within a 4 AU semi-major axis interval around 39.45 AU. Twenty-two objects have well determined orbits and 46 objects have the eccentricity assumed. The latter group represents orbits with small observational arcs and orbital elements that are very imprecise. Indeed, we have verified that most orbits of the first group are stable inside the 2:3 MMR and that most orbits of the second group are unstable on unrealistically short time intervals.

Next, we have integrated the 22 objects of the first group and Pluto (as massless test particles) with four giant planets for 10^7 years using the symmetric multi-step integrator. Periods shorter than 1200 years were suppressed by digital filtering.

Table III shows the orbital characteristics of Pluto and 15 Plutinos that were found on stable orbits over 10^7 years inside the 2:3 MMR. Figure 11 shows the maxima and minima of their a , e , and i on 10^7 years (the plot of the LCE was adapted from Figs. 2a and 8a to a grey scale). In Fig. 11a, we plot a pair of

TABLE III
Pluto and KBOs Found in the 2:3 MMR

No.	Designation	Distance	A_σ	A_ω	a_{\min}	a_{\max}	e_{\min}	e_{\max}	i_{\min}	i_{\max}
1	Pluto	16.7	84.8	22.8	39.297	39.622	0.214	0.270	14.40	17.40
2	1993 RO	11.5	123.0	—	39.195	39.711	0.188	0.210	1.96	6.01
3	1993 SB	20.1	65.2	—	39.311	39.618	0.308	0.324	1.48	4.98
4	1993 SC	14.5	76.7	—	39.315	39.597	0.172	0.196	3.77	8.01
5	1994 JR1	11.5	94.5	—	39.279	39.621	0.111	0.138	1.14	5.73
6	1994 TB	17.6	54.5	73.2	39.358	39.555	0.178	0.317	12.10	21.30
7	1995 HM5	16.1	72.4	—	39.317	39.606	0.206	0.268	2.86	9.84
8	1995 QY9	10.5	132.0	—	39.143	39.789	0.249	0.267	3.61	7.75
9	1995 QZ9	15.0	41.5	—	39.396	39.501	0.115	0.178	17.20	21.80
10	1995 RR20	10.4	130.0	—	39.180	39.731	0.171	0.197	2.49	7.68
11	1996 SZ4	15.0	91.5	—	39.274	39.654	0.206	0.262	3.00	9.83
12	1996 TP66	21.7	17.2	—	39.409	39.510	0.314	0.334	5.49	9.21
13	1996 TQ66	13.8	27.6	—	39.413	39.472	0.088	0.130	13.10	16.60
14	1997 QJ4	15.0	102.0	35.1	39.259	39.665	0.207	0.263	14.10	18.50
15	1998 HK151	17.6	47.3	79.2	39.366	39.551	0.218	0.259	0.87	8.72
16	1998 HQ151	19.6	43.6	—	39.370	39.551	0.270	0.314	10.70	14.60

Note. Minimum distances to Neptune are shown in column 3 (Distance). Angles are in degrees; distances and semi-major axes are in astronomical units. Minimum and maximum filtered orbital elements were computed for 10^7 years.

secular resonance $g-s+g_8-s_8$

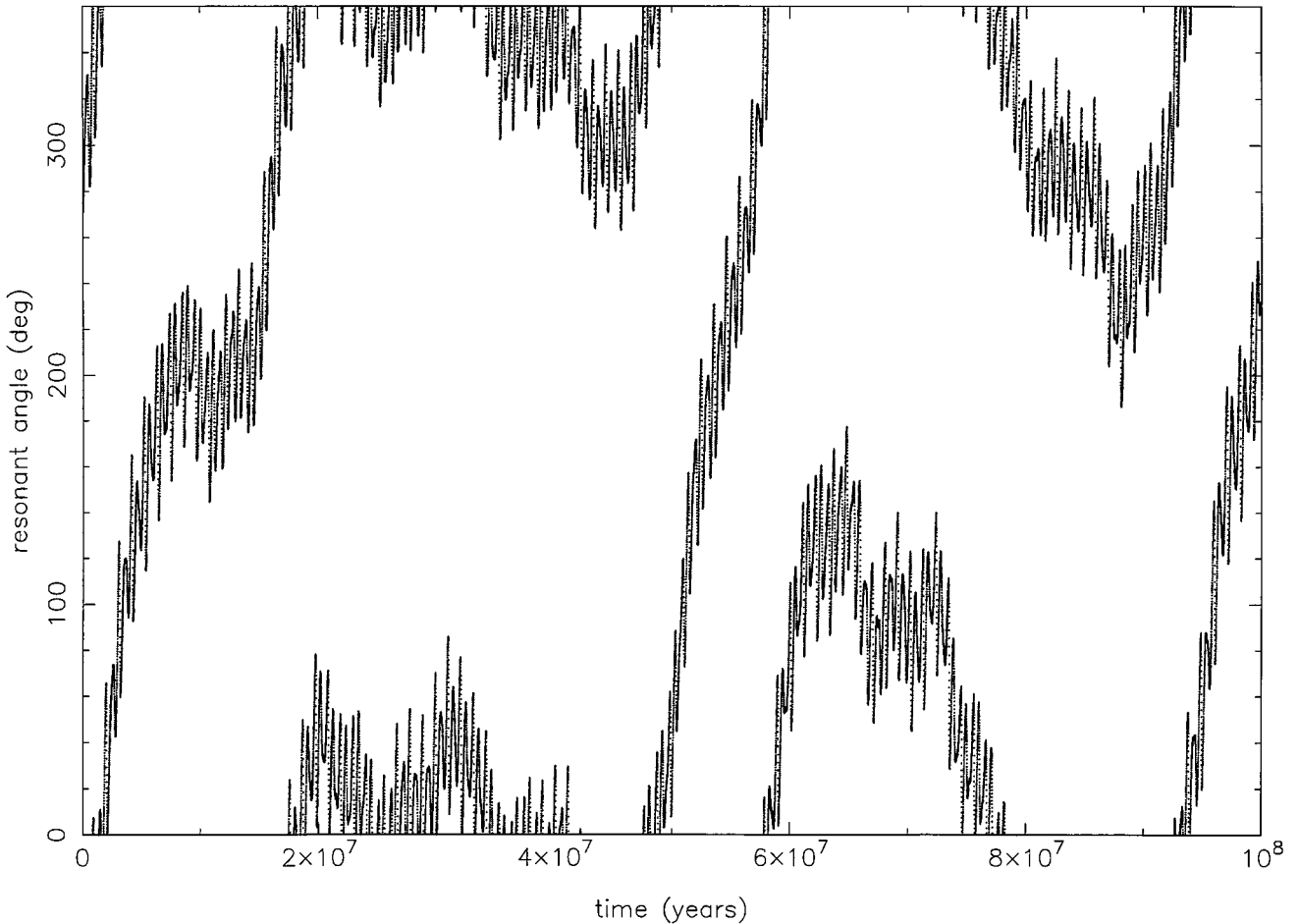


FIG. 10. The evolution of the angle $\omega - \varpi_N + \Omega_N$ of a test particle located in the secular resonance $g - s + g_8 - s_8$.

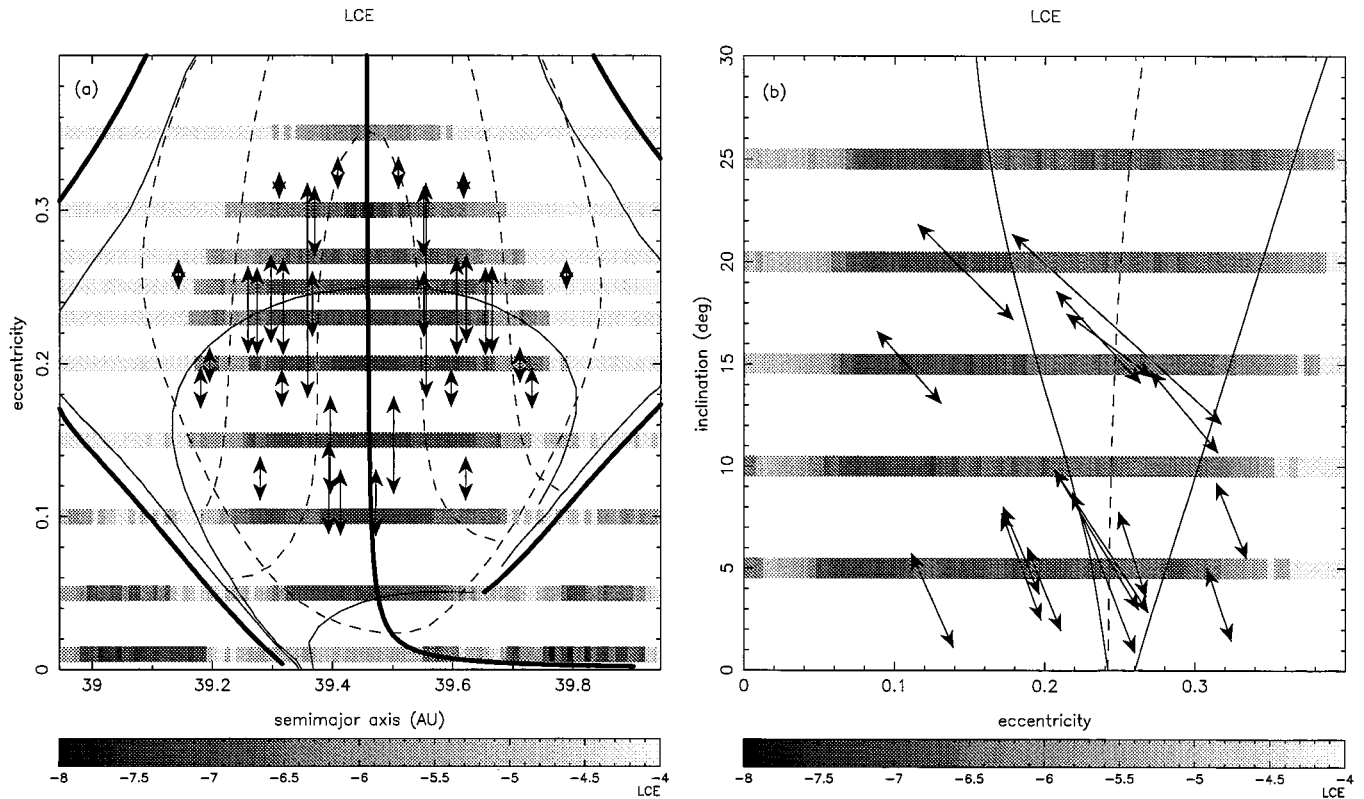


FIG. 11. The orbital distribution of Plutinos. The arrows indicate the maxima and minima of the orbital elements in 10^7 years (Table III). Note the two groups in (b) characterized by small ($\sim 5^\circ$) and large ($\sim 16^\circ$) inclinations.

two-headed arrows per object, one at the minimum and one at the maximum values of a . Each of these arrows connect the minimum and maximum values of the object's e (Table III). In Fig. 11b there is only one arrow per object connecting the two points with coordinates (e_{\min}, i_{\max}) and (e_{\max}, i_{\min}) , respectively. For Pluto and Plutinos in the Kozai resonance, where the evolutions of e and i are correlated, the arrows in Fig. 11b approximately indicate the true variation of e and i . For Plutinos outside the Kozai resonance, these arrows delimit the extension of a rectangle where e and i evolve.

Figure 11a shows that Plutinos are well accommodated within the central stable space of the 2:3 MMR. Only 1995 QY9 and 1995 RR20 have large resonant amplitudes ($A_\sigma = 132^\circ$ and 130° , respectively), and if their orbital elements were well determined from observations, these objects should escape from the resonance within 10^8 years. Moreover, 1993 RO is on the border between the marginally unstable and strongly unstable regions with $A_\sigma = 123^\circ$, $e = 0.2$, and small i . The orbital elements of these Plutinos derived from observations should be slightly incorrect because, otherwise, the suggested escape rate from the 2:3 MMR would be unrealistically large (more than 5% of the current population per 10^8 years).

There are two unpopulated stable regions, one at small eccentricities ($0.05 \leq e < 0.1$) and the other in the center ($39.35 < a < 39.55$ AU and $0.15 < e < 0.3$). Note that for $e > 0.1$ there

are no Plutinos with A_σ smaller than the amplitude corresponding to the 5:1 three-body resonance.

The void region at small e cannot be a consequence of the observational selection effect, because many KBOs on orbits with $e < 0.1$ have been found at larger heliocentric distances ($42 < a < 45$ AU) than the 2:3 MMR. Note that a similarly unpopulated region exists at $37 < a < 39$ AU and $e < 0.05$ (one can partially see it in Fig. 11a just outside the left separatrix of the 2:3 MMR) and has been discussed by Duncan *et al.* (1995). It was suggested by them that the clearing occurred there during the early stages of the Solar System formation. The two main scenarios of how this may happened are the planetary migration/sweeping resonances scenario of Malhotra (1995) and the excitation of e (and i) by large planetesimals suggested by Petit *et al.* (1999). It is possible that the void region at small e of the 2:3 MMR has a similar origin.

The void central region at small $A_\sigma < 60^\circ$ is a real puzzle. It is true that the resonant bodies with small A_σ are expected to be less numerous than the ones with large A_σ as they occupy a relatively small volume in the phase space, but, on the other hand, the observed void at small A_σ in the 2:3 MMR is more pronounced than what would be inferred from the above argument. If confirmed by future observations, this void may be a consequence of the scattering effect of Pluto (Nesvorný *et al.* 2000).

One can clearly distinguish two groups with different inclinations in Fig. 11b. There are 10 low-inclination objects ($i_{\max} < 10^\circ$ and average of 5°) and 6 high-inclination objects (including Pluto— $i_{\min} > 10^\circ$ and average of 16°). The latter group was conjectured to be a remnant of the collision in which the Pluto–Charon binary formed (Stern *et al.* 1999). Indeed, there is no dynamic reason for the intermediate inclinations being underpopulated.

Apart from Pluto, only one object—1997 QJ4—was found with stable libration in the Kozai resonance. It has $A_\omega \sim 35^\circ$. Two other potential potential objects in the Kozai resonance—1994 TB and 1998 HK151—have large A_ω and evolve within 5×10^7 years to the separatrices of the Kozai resonance. 1997 QJ4 is the only KBO discovered until now that shares the 2:3 and Kozai resonances with Pluto. This makes this body an interesting object for future spectroscopic observations as it might be one of few low-velocity ejecta of Pluto–Charon binary formation event that survived the scattering effect of Pluto until present times. Indeed, Nesvorný *et al.* (2000) showed that Pluto’s gravitational sweeping effect can efficiently remove the objects from Pluto’s surroundings.

9. CONCLUSIONS

The dynamics of the 2:3 mean motion resonance with Neptune have been studied in this paper. We have numerically computed the maximum LCE, frequencies, and measures of chaotic diffusion on a grid of a , e , i . This allowed us to determine the most important inner resonances. Apart from previously known resonances, we have found the 4:1 and 5:1 three-body resonances (the commensurabilities between the resonant period and the period of the inequality 2:1 between Uranus and Neptune) and the secular resonance $g - s + g_8 - s_8$. The 4:1 three-body resonance is important because it is located on the margin of the stable region of the 2:3 MMR.

We have defined the marginally unstable region as the place where the escape rate to Neptune–crossing orbits at $t = 4$ Byr is more than 1% of the initial population per 1 Byr. This definition was motivated by the need for identification of the area that is an active source of Jupiter–family comets in present times. We have shown that the marginally unstable area has a typical width of several tens of degrees in A_σ and estimated the present relative flux of escaping objects from the 2:3 MMR to be 1.7% of the current resonant population per billion years. This value, calibrated by the number of active and extinct Jupiter–family comets and their lifetimes, led to the estimate of 6×10^8 objects corresponding to $H_T < 9$ ($D > 1\text{--}3$ km) currently in the 2:3 MMR. This number is only an upper limit if the contribution of the Scattered Disk to the flux of ecliptic comets is important or if other processes than purely dynamic ones (driven by four outer planets) play an important role.

The orbital distribution of observed Plutinos falls within the limits of orbital stability in A_σ and e . Low- A_σ orbits for $0.15 < e < 0.3$ and low- e orbits ($e < 0.1$) are stable but do not seem

to be well sampled by known Plutinos. These voids may be either dynamically primordial or a consequence of collisions and dynamic scattering in the resonance. Two groups with $i \sim 5^\circ$ and $i \sim 16^\circ$ were identified. If the latter one is a product of the Pluto–Charon binary formation event then 1997 QJ4 is a good candidate for a member of Pluto’s family.

In a second paper (Nesvorný and Roig, 2000), we extend the present analysis to the 1:2, 3:4 and fine mean motion resonances in the trans-Neptunian region.

ACKNOWLEDGMENTS

This research was sponsored by the São Paulo State Science Foundation FAPESP. Some of the numerical simulations were performed using the facilities of the São Paulo University computer center LCCA in the frame of the project “Asteroid Resonant Dynamics and Chaos.” We thank Fabrice Thomas for supplying us with his semi-numerical determination of resonant and secular frequencies in the 2:3 MMR. We also thank Carl Murray and Edward Thommes for valuable referees’ reports that helped us improve the manuscript.

REFERENCES

- Benettin, G., L. Galgani, and J. M. Strelcyn 1976. Kolmogorov entropy and numerical experiments. *Phys. Rev. A* **14**, 2338–2345.
- Duncan, M. J., and H. F. Levison 1997. A disk of scattered icy objects and the origin of Jupiter-family comets. *Science* **276**, 1670–1672.
- Duncan, M., H. F. Levison, and S. M. Budd 1995. The dynamical structure of the Kuiper Belt. *Astron. J.* **110**, 3073–3081.
- Edgeworth, K. E. 1949. The origin and evolution of the Solar System. *MNRAS* **109**, 600–609.
- Farinella, P., D. Davis, and S. A. Stern 2000. Formation and collisional evolution of the Edgeworth–Kuiper Belt. In *Protostars and Planets IV* (V. Mannings, A. Boss, and S. Russell, Eds.), pp. 1255–1282. Univ. of Arizona Press, Tucson, AZ.
- Fernández, J. A. 1980. On the existence of a comet belt beyond Neptune. *MNRAS* **192**, 481–491.
- Ferraz-Mello, S. 1994. Dynamics of the asteroidal 2/1 resonance. *Astron. J.* **108**, 2330–2337.
- Ferraz-Mello, S., T. A. Michtchenko, and F. Roig 1998. The determinant role of Jupiter’s Great Inequality in the depletion of the Hecuba gap. *Astron. J.* **116**, 1491–1500.
- Hahn, J. M., and R. Malhotra 1999. Orbital evolution of planets embedded in a planetesimal disk. *Astron. J.* **117**, 3041–3053.
- Henrard, J. 1990. A semi-numerical perturbation method for separable Hamiltonian systems. *Celest. Mech. Dynam. Astron.* **49**, 43–67.
- Holman, M., and J. Wisdom 1993. Dynamical stability in the outer Solar System and the delivery of short period comets. *Astron. J.* **105**, 1987–1999.
- Jewitt, D., and J. Luu 1993. Discovery of the candidate Kuiper Belt object 1992 QB1. *Nature* **362**, 730–732.
- Jewitt, D., J. Luu, and C. Trujillo 1998. Large Kuiper Belt objects: The Mauna Kea 8K CCD survey. *Astron. J.* **115**, 2125–2135.
- Kinoshita, H., and H. Nakai 1984. Motions of the perihelions of Neptune and Pluto. *Celest. Mech. Dynam. Astron.* **34**, 203–217.
- Knežević, Z., A. Milani, P. Farinella, Ch. Froeschlé, and C. Froeschlé 1991. Secular resonances from 2 to 50 AU. *Icarus* **93**, 316–330.
- Kuiper, G. P. 1951. The origin of the Solar System. In *Astrophysics: A Topical Symposium* (J. A. Hynek, Ed.), pp. 357–406. McGraw–Hill, New York.
- Laskar, J. 1988. Secular evolution of the Solar System over 10 million years. *Astron. Astrophys.* **198**, 341–362.

- Laskar, J. 1994. Large-scale chaos in the Solar System. *Astron. Astrophys.* **287**, L9–L12.
- Laskar, J. 1999. Introduction to frequency map analysis. In *Hamiltonian Systems with Three or More Degrees of Freedom* (C. Simó, Ed.), pp. 134–150. Kluwer Academic, Dordrecht.
- Levison, H. F., and M. Duncan 1993. The gravitational sculpting of the Kuiper belt. *Astrophys. J.* **406**, L35–L38.
- Levison, H. F., and M. Duncan 1997. From the Kuiper belt to Jupiter-family comets: The spatial distribution of ecliptic comets. *Icarus* **127**, 13–32.
- Levison, H. F., Duncan, M. J., Zahnle, K., M. Holman, and L. Dones 2000. Planetary impact rates from ecliptic comets. *Icarus* **143**, 415–420.
- Levison, H. F., and S. A. Stern 1995. Possible origin and early dynamical evolution of the Pluto–Charon binary. *Icarus* **116**, 315–339.
- Liou, J. C., and R. Malhotra 1997. Depletion of the outer asteroid belt. *Science* **275**, 375–377.
- Malhotra, R. 1995. The origin of Pluto's orbit: Implications for the Solar System beyond Neptune. *Astron. J.* **110**, 420–429.
- Malhotra, R. 1996. The phase space structure near Neptune resonances in the Kuiper belt. *Astron. J.* **111**, 504–516.
- Malhotra, R. 1997. Implications of the Kuiper Belt structure for the Solar System. *ACM Conference 1996*, Versailles, France. Unpublished.
- Moons, M., A. Morbidelli, and F. Migliorini 1998. Dynamical structure of the 2/1 commensurability with Jupiter and the origin of the resonant asteroids. *Icarus* **135**, 458–468.
- Morbidelli, A. 1996. The Kirkwood gap at the 2/1 commensurability with Jupiter: New numerical results. *Astron. J.* **111**, 2453–2461.
- Morbidelli, A. 1997. Chaotic diffusion and the origin of comets from the 2/3 resonance in the Kuiper belt. *Icarus* **127**, 1–12.
- Morbidelli, A., and C. Froeschlé 1995. On the relationship between Lyapunov times and macroscopic instability times. *Celest. Mech. Dynam. Astron.* **63**, 227–239.
- Morbidelli, A., and D. Nesvorný 1999. Numerous weak resonances drive asteroids toward terrestrial planets orbits. *Icarus* **139**, 295–308.
- Morbidelli, A., F. Thomas, and M. Moons 1995. The resonant structure of the Kuiper Belt and the dynamics of the first five trans-Neptunian objects. *Icarus* **118**, 322–340.
- Murray, N., and M. Holman 1997. Diffusive chaos in the outer asteroid belt. *Astron. J.* **114**, 1246–1259.
- Nesvorný, D., and S. Ferraz-Mello 1997a. Chaotic diffusion in the 2/1 asteroidal resonance: An application of the frequency map analysis. *Astron. Astrophys.* **320**, 672–680.
- Nesvorný, D., and S. Ferraz-Mello 1997b. On the asteroidal population of the first-order jovian resonances. *Icarus* **130**, 247–258.
- Nesvorný, D., and F. Roig 2000. Mean motion resonances in the trans-neptunian region. II. The 1:2, 3:4 and fine mean motion resonances. *Icarus*, submitted for publication.
- Nesvorný, D., F. Roig, and S. Ferraz-Mello 2000. Close approaches of trans-Neptunian objects to Pluto have left observable signatures on their orbital distribution. *Astron. J.* **119**, 953–969.
- Oseledec, V. I. 1968. A multiplicative ergodic theorem: Lyapunov characteristic numbers for dynamical systems. *Trans. Moscow Math. Soc.* **19**, 197–231.
- Petit, J. M., A. Morbidelli, and G. Valsecchi 1999. Large scattered planetesimals and the excitation of the small body belts. *Icarus* **141**, 367–387.
- Press, W., S. Teukolsky, W. Vetterling, and B. Flannery 1992. *Numerical Recipes: The art of scientific computing*. Cambridge Univ. Press, Cambridge, UK.
- Quinlan, G., and S. Tremaine 1990. Symmetric multistep methods for the numerical integration of planetary orbits. *Astron. J.* **100**, 1694–1700.
- Quinn, T., S. Tremaine, and M. Duncan 1991. A three million year integration of the Earth's orbit. *Astron. J.* **101**, 2287–2305.
- Šidlichovský, M., and D. Nesvorný 1997. Frequency modified Fourier transform and its applications to asteroids. *Celest. Mech. Dynam. Astron.* **65**, 137–148.
- Stern, S. A., R. Canup, and D. Durda 1999. Pluto's family: Debris from the binary-forming collision in the 2:3 resonance? In *30th Annual Lunar and Planetary Science Conference, Houston, Texas*, abstract 1213.
- Sussman, G., and J. Wisdom 1988. Numerical evidence that the motion of Pluto is chaotic. *Science* **241**, 433–437.